Cell Reports

Article

Candida auris uses metabolic strategies to escape and kill macrophages while avoiding robust activation of the NLRP3 inflammasome response

Graphical abstract

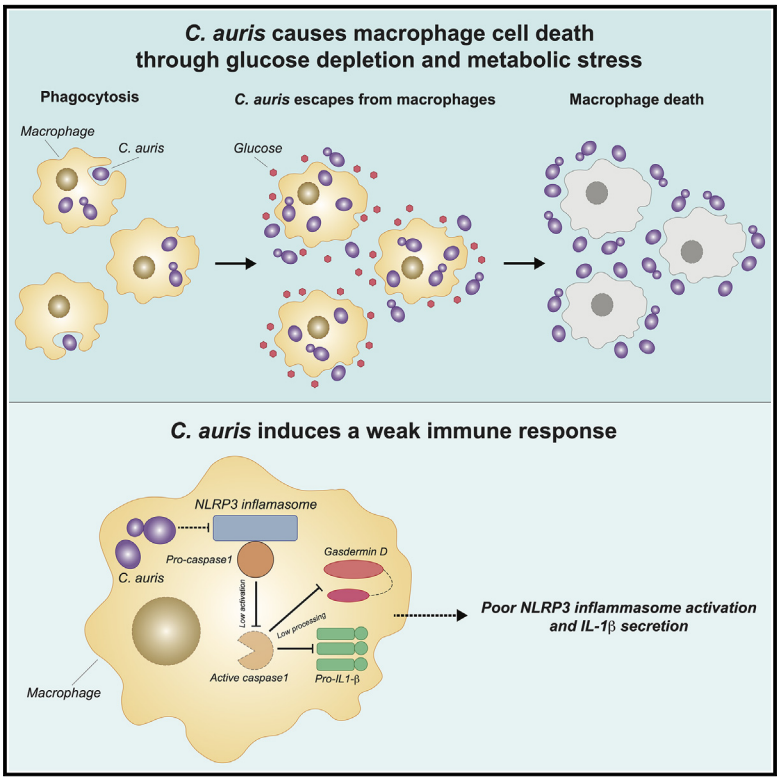

Authors

Harshini Weerasinghe, Claudia Simm, Tirta Mario Djajawi, ..., Kate E. Lawlor, Ronen Ben-Ami, Ana Traven

Correspondence

ana.traven@monash.edu

In brief

The pathogen *Candida auris* is phagocytosed by macrophages during innate immune responses. Weerasinghe et al. show that *C. auris* evades macrophages by escaping and depleting glucose, which triggers macrophage cell death. Despite causing macrophage metabolic dysfunction and death, *C. auris* does not activate robust NLRP3-inflammasome responses, thereby evading antimicrobial inflammation.

Highlights

- *C. auris* escapes from macrophages
- *C. auris* kills macrophages by depleting glucose and causing host metabolic stress
- *C. auris* glycolysis facilitates yeast proliferation *in vivo* and macrophage killing
- *C. auris*-infected macrophages trigger poor NLRP3 inflammasome responses

Weerasinghe et al., 2023, Cell Reports *42*, 112522
May 30, 2023
https://doi.org/10.1016/j.celrep.2023.112522

CellPress

Cell Reports

CellPress
OPEN ACCESS

Article

Candida auris uses metabolic strategies to escape and kill macrophages while avoiding robust activation of the NLRP3 inflammasome response

Harshini Weerasinghe,[1,2] Claudia Simm,[1,2] Tirta Mario Djajawi,[3,4] Irma Tedja,[1,2] Tricia L. Lo,[1,2] Daniel S. Simpson,[5,6] David Shasha,[7,8] Naama Mizrahi,[7] Françios A.B. Olivier,[1,2,5] Mary Speir,[3,4,9] Kate E. Lawlor,[3,4] Ronen Ben-Ami,[7,8] and Ana Traven[1,2,10,*]

[1]Infection Program and the Department of Biochemistry and Molecular Biology, Biomedicine Discovery Institute, Monash University, Clayton, VIC 3800, Australia
[2]Centre to Impact AMR, Monash University, Clayton, VIC 3800, Australia
[3]Centre for Innate Immunity and Infectious Diseases, Hudson Institute of Medical Research, Clayton, VIC 3168, Australia
[4]Department of Molecular and Translational Science, Monash University, Clayton, VIC 3168, Australia
[5]The Walter and Eliza Hall Institute of Medical Research, Parkville, VIC 3052, Australia
[6]The Department of Medical Biology, University of Melbourne, Parkville, VIC 3010, Australia
[7]Infectious Diseases Unit, Tel Aviv Sourasky Medical Centre, Tel Aviv, Israel
[8]Faculty of Medicine, Tel Aviv University, Tel Aviv, Israel
[9]Present address: Noxopharm Ltd, The Zenith, 821 Pacific Hwy, Chatswood, NSW 2067, Australia
[10]Lead contact
*Correspondence: ana.traven@monash.edu
https://doi.org/10.1016/j.celrep.2023.112522

SUMMARY

Metabolic adaptations regulate the response of macrophages to infection. The contributions of metabolism to macrophage interactions with the emerging fungal pathogen *Candida auris* are poorly understood. Here, we show that *C. auris*-infected macrophages undergo immunometabolic reprogramming and increase glycolysis but fail to activate a strong interleukin (IL)-1β cytokine response or curb *C. auris* growth. Further analysis shows that *C. auris* relies on its own metabolic capacity to escape from macrophages and proliferate *in vivo*. Furthermore, *C. auris* kills macrophages by triggering host metabolic stress through glucose starvation. However, despite causing macrophage cell death, *C. auris* does not trigger robust activation of the NLRP3 inflammasome. Consequently, inflammasome-dependent responses remain low throughout infection. Collectively, our findings show that *C. auris* uses metabolic regulation to eliminate macrophages while remaining immunologically silent to ensure its own survival. Thus, our data suggest that host and pathogen metabolism could represent therapeutic targets for *C. auris* infections.

INTRODUCTION

Drug-resistant microbial pathogens threaten human health and medicine. The yeast *Candida auris* is one such pathogen, which emerged in clinical settings a little over a decade ago as a cause of bloodstream infections with high associated mortality.[1,2] *C. auris* shows intrinsic resistance to front-line antifungal drugs, common multidrug resistance, and even pan-drug resistance in some cases, which is especially problematic given the small number of available antifungal therapies.[1–4]

In addition to treatment with antifungal drugs, the patient's own immune system attempts to control fungal infections.[5] We are only beginning to understand how *C. auris* overcomes immunity to establish infection. Mannan in the *C. auris* cell wall has been implicated in hiding the immunostimulatory cell wall component β-glucan.[6] It has been suggested that mannan shields *C. auris* from recognition by macrophages and neutrophils, thereby reducing fungal killing and curbing proinflammatory cytokine production.[6,7] However, another study concluded the opposite, showing that *C. auris* mannan induces more potent proinflammatory responses in human peripheral blood mononuclear cells (PBMCs) compared with the common fungal pathogen *Candida albicans*.[8]

In addition to modulation of cell surface antigens, immune evasion by microbial pathogens involves metabolic adaptations to changing nutrient conditions in immune phagocytes.[9] Moreover, changes in the metabolism of immune cells have emerged as major factors regulating host responses to pathogens.[9–12] Based on these studies, it has been proposed that metabolic interventions could promote beneficial immune, tissue, and organ responses that protect host health during infection.[9,11,13] Clinical data backs this proposition, as maintaining metabolic homeostasis is important for improving outcome in patients suffering from infections and sepsis.[14,15]

As major reservoirs for the replication of microbial pathogens, macrophages have been studied for metabolic regulation during

infection. Bacterial or fungal challenges cause a shift in macrophage metabolism whereby microbial killing and cytokine production are promoted by increased glycolysis, reduced mitochondrial respiration and changes to the tricarboxylic acid (TCA) cycle.[16–23] Pathogens can counter these host metabolic changes in several ways, for example by competitively using metabolites produced by macrophages for their own growth[24,25] or by modulating immune cell viability and function through nutrient competition.[26–28] The metabolic mechanisms that control infection survival can vary between pathogens and therefore understanding is required across diverse infections.[9]

In this study, we establish a pivotal role for metabolic regulation in macrophage evasion by *C. auris.* Our study provides a framework for understanding how metabolism could be harnessed to modulate *C. auris* immune interactions that control infections.

RESULTS

C. auris escapes from macrophages

Few studies have been published on the interaction between *C. auris* and macrophages. Therefore, to define how *C. auris* affects macrophage responses, we first assessed our strain (470121, clade I) for phagocytic uptake and fate in murine bone marrow-derived macrophages (BMDMs).

C. auris was phagocytosed by BMDMs, with an average of 3.17 yeast per macrophage counted 1 h post challenge with an MOI of 3 (Dataset S1). The number of yeast cells/macrophage exceeding the MOI could be due to yeast replication inside macrophages (Figure 1A). This result is consistent with our previous work with a different *C. auris* isolate and the work of Bruno et al.[8,29] Therefore, replication in macrophages *in vitro* is a general capability of *C. auris* strains.

At 8–10 h post challenge, *C. auris* escaped from macrophages, as evident by the accumulation of yeast cells in the surrounding medium and a sharp increase in extracellular colony-forming units (CFUs) (Figures 1A, 1B, and S1A; Video S1). Several escape events were observed from individual macrophages (Video S2). There was no morphological change associated with the escape; i.e., *C. auris* remained in yeast form throughout the experiment (Figure 1B; Videos S1 and S2). Replication within macrophages and *C. auris* escape occurred in several carbon sources (glucose, galactose, and mannose) (Figure S1B). Distinct carbon sources could influence both host and pathogen physiology. Despite the carbon sources promoting comparable intracellular *C. auris* CFUs (resulting from replication in macrophages), the extracellular CFUs (resulting from replication in medium after escape) showed a statistically significant difference for glucose and mannose compared with the condition lacking glucose (10 h) (Figure S1C). CFUs in galactose were not statistically different to no glucose (Figure S1C). This correlated with the differing abilities of our *C. auris* strain to utilize these carbon sources: *C. auris* growth was faster in glucose and mannose compared with media lacking in glucose (Figure S1C).

Despite egress and abundant extracellular yeast growth being evident at 10 h post *C. auris* infection (Figure 1A), there was no associated increase in lactate dehydrogenase (LDH) release as a measure of macrophage plasma membrane damage (Figure 1C). Therefore, *C. auris* is able to egress from macrophages to promote dissemination, but this is not associated with widespread macrophage lysis.

C. auris kills macrophages

Extending the time course showed that, at 24 h post infection, LDH release increased significantly from *C. auris*-infected macrophages (Figure 1C). This result indicated that, although the initial yeast escape does not trigger macrophage lysis, lysis does occur at later time points. To further understand the dynamics of macrophage lysis and killing by *C. auris*, we employed our live-cell imaging platform. This imaging platform uses nuclear staining with the dye DRAQ7 as a measure of macrophage membrane permeabilization and cell death and quantifies these events at single-cell level in macrophage populations *in vitro*.[30] Live-cell imaging confirmed that macrophages survived the initial escape of *C. auris* and did not succumb for several hours afterward (Figure 2A; Video S1). Rapid macrophage membrane permeabilization initiated at around 16–18 h after challenge. It reached almost 100% of DRAQ7-positive macrophages by 24 h with an MOI of 6 and close to 70% with MOI of 3 (Figure 2A). As pH levels were maintained (pH 6–7) during infection (Figure S1D), the observed macrophage cell death is unlikely to be caused by acidification of the medium.

It was possible that macrophage cell death was not only triggered by escaped *C. auris* but also by residual extracellular yeast that had evaded phagocytosis. To address this, we killed non-phagocytosed yeast by adding 25 μg/mL of the membrane-impermeable calcofluor white after phagocytosis. At 25 μg/mL calcofluor white inhibits *C. auris* growth in media by 99.98% (Figure S1E). After 1 h, calcofluor white was washed off, and then the infection was allowed to proceed to enable *C. auris* escape and macrophage killing. Treatment with calcofluor white did not cause any difference in macrophage cell death kinetics (Figure 2B). This indicates that, if there are any *C. auris* cells that evade phagocytosis, they do not majorly contribute to macrophage killing. Heat-killed *C. auris* (which neither replicates nor escapes) was also unable to cause macrophage cell death (Figure 2C). Additionally, adding the antifungal drug caspofungin at 6 h after challenge (by which time *C. auris* escaped and extracellular replication occurs) prevented macrophage cell death (Figure 2D). The escape and killing of mouse macrophages by *C. auris* (Figure 2A) were recapitulated in human monocyte-derived macrophages (hMDMs). Here also, actively replicating *C. auris* was required, as treatment with caspofungin inhibited cell death of hMDMs (Figure 2E). Together, these experiments indicate that *C. auris* needs to escape and then actively replicate extracellularly to kill macrophages.

We wanted to further ascertain whether the ability to escape and kill macrophages *in vitro* was conserved between isolates belonging to distinct genomic clades.[31] *C. auris* strains from clades I–IV were obtained from the Centers for Disease Control and Prevention (CDC) and used in time-lapse imaging assays quantifying macrophage viability. The phagocytic indices for these strains were comparable (Figure S2A), and the escape and killing of macrophages was observed across clades I–IV (Figure 2F; Video S3). There were, however, differences in the kinetics. The clade IV strain B11244 triggered macrophage cell death 2 h earlier than all other clades (starting at 14–16 h), while

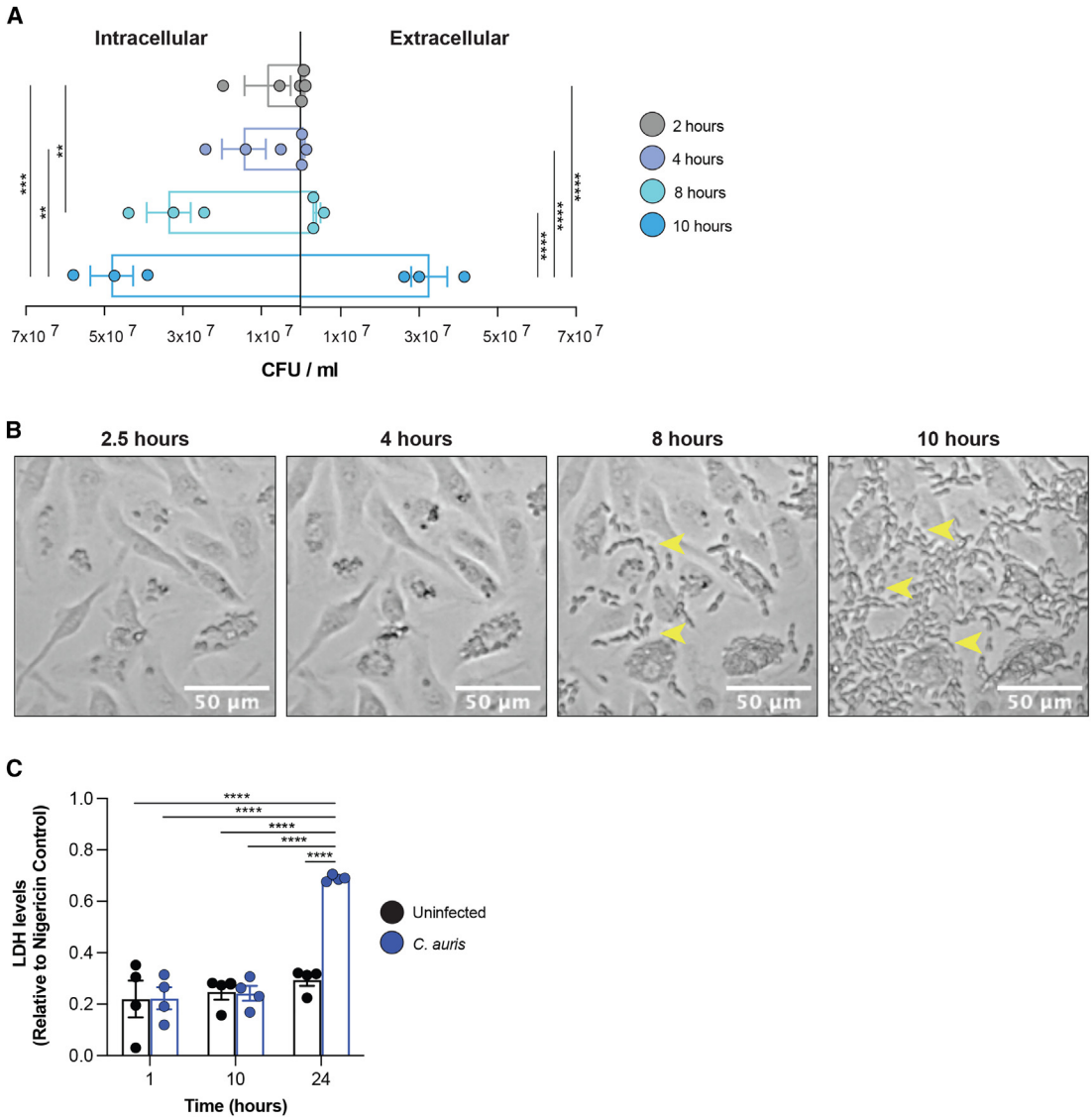

Figure 1. *C. auris* escapes from macrophages

(A) Quantitation of colony forming units (CFUs) of *C. auris* 470121 for intracellular growth in macrophages (BMDMs) and extracellular growth in the surrounding medium (MOI 3). Supernatants and macrophage lysates were plated at 2, 4, 8, and 10 h post challenge and CFUs counted after 2 days at 30°C. Shown are mean values and SEM from three independent experiments (one-way ANOVA Bonferroni's multiple comparison test, ***p ≤ 0.001, ****p ≤ 0.0001). Only statistically significant comparisons are indicated.

(B) Microscopy images from Video S1 of *C. auris* infecting and escaping BMDMs at 2, 4, 8, and 10 h post challenge. Images are magnifications of a section of the field of view (shown in Figure S1A). Yellow arrowheads indicate yeast cells that have escaped (8- and 10-h time point). Video S2 shows escape events in individual macrophages.

(C) Measurements of lactate dehydrogenase (LDH) release of uninfected and *C. auris*-infected macrophages at 1, 10, and 24 h post challenge. The NLRP3 inflammasome activator nigericin causes widespread macrophage lysis and was used as a control. Values were expressed relative to LDH release from nigericin-treated macrophages. Shown are mean values and SEM from four independent experiments (two-way ANOVA Bonferroni's multiple comparison test, ****p ≤ 0.0001). Only statistically significant comparisons are indicated.

the clade II strain B11220 and the clade III strain B11241 were the slowest, showing a delay of 2 or 4 h respectively (Figure 2F). Although it is not possible to extrapolate growth rates *in vitro* to those during macrophage infections, we note that clade II and clade III isolates were not only the slowest to kill macrophages but also the slowest growing *in vitro* (Figure S2B). However, growth rates *in vitro* did not correlate to the speed of macrophage killing for all strains, as B11244 was the fastest in triggering macrophage cell death, but it was not the fastest growing strain of the group (Figure S2B). Collectively, our findings show that the ability of *C. auris* to kills macrophages is conserved across genetic clades.

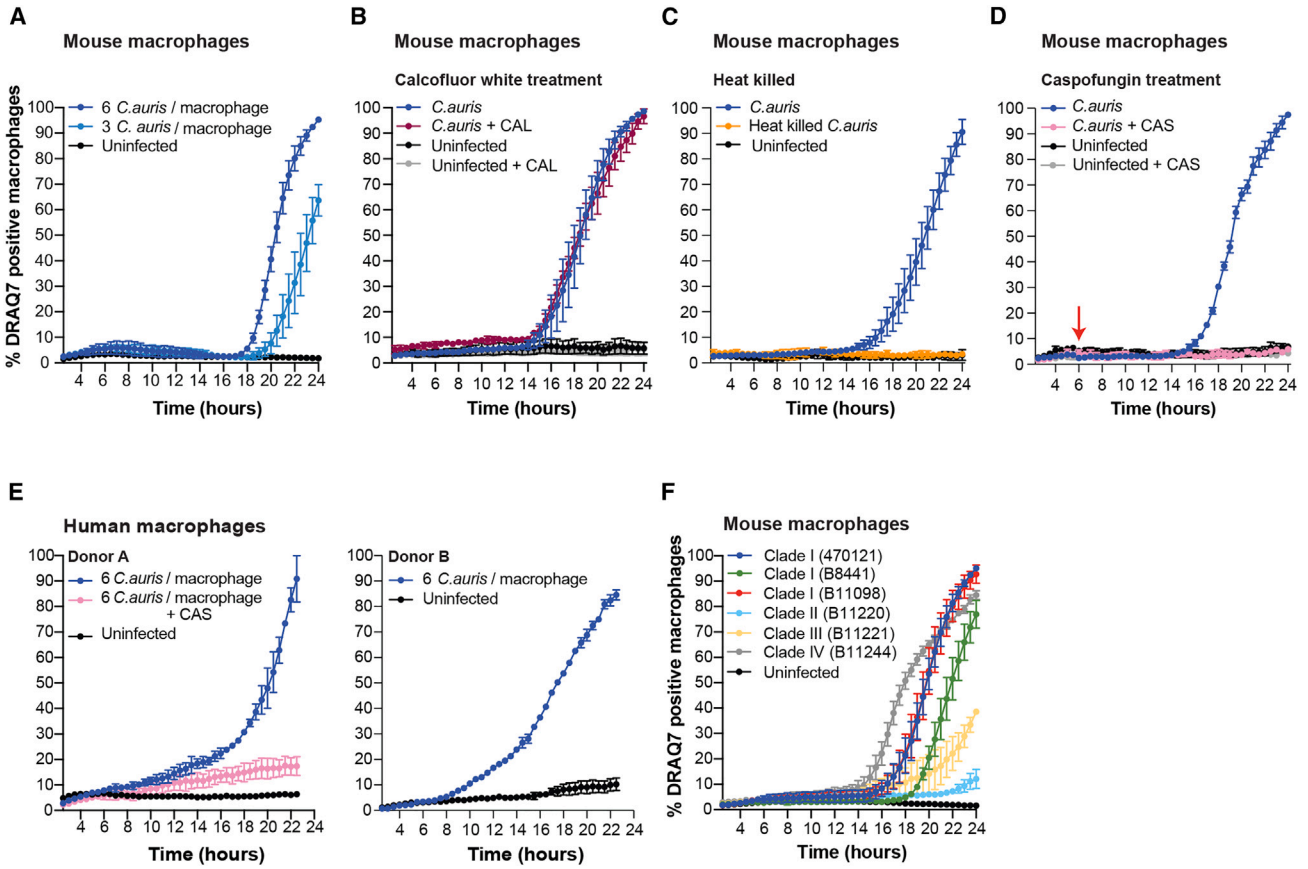

Figure 2. *C. auris* kills mouse and human macrophages

(A) BMDMs were challenged with *C. auris* 470121 (MOI 3 or 6) and imaged. Macrophage membrane permeabilization was determined using the membrane-impermeable dye DRAQ7 and DRAQ7-positive nuclei counted over time. Shown are the mean and SEM for three independent experiments.

(B) Same as (A) but with the addition of 25 μg/mL calcofluor white (CAL) at 1 h post infection to kill non-phagocytosed *C. auris* (see Figure S1D). CAL was applied for 1 h, followed by its removal and continuing with live-cell imaging. The MOI was 6. Shown are the mean and SEM for three independent experiments.

(C) Same as (B), but BMDMs were challenged with live versus heat-killed *C. auris*.

(D) Same as (B), but with or without 125 ng/mL caspofungin (CAS) added at 6 h post infection (red arrow). This experiment was analyzed together with the two nutrients spike experiments from Figure 3C. As such, the standard medium (blue graph) and uninfected macrophage data is the same here and in Figure 3C. Shown are the mean and SEM for three independent experiments.

(E) Same as (A), but human monocyte-derived macrophages (hMDMs) from two independent healthy donors (A and B) were used. *C. auris* strain was 470121, MOI 6. For donor A, 125 ng/mL caspofungin was added to the media after phagocytosis. Donor A and B are two independent experiments; in each, we show the mean and SEM values for two independent experiments.

(F) Same as (A), but mouse BMDMs were challenged with *C. auris* isolates belonging to clades I–IV (MOI 6). Shown are the mean values and SEM for three independent experiments.

C. auris kills macrophages by causing metabolic stress

The findings in Figure 2 suggested that active proliferation of *C. auris* was important for inducing macrophage death. We hypothesized two possible mechanisms: (1) *C. auris* is competing for nutrients required to sustain macrophage viability, or (2) *C. auris* is secreting a compound toxic to macrophages.

Central carbon metabolism is critical for infected macrophages, reviewed in Traven and Naderer.[9] Therefore, to test the nutrient competition hypothesis, we supplemented macrophage media with metabolites that feed into central carbon metabolism (Figure 3A) and asked if they could rescue macrophages from *C. auris*-induced cell death. Supplementation of glucose or pyruvate delayed death of *C. auris*-infected macrophages, while supplementation of arginine, glutamine, or acetate did not (Figure 3B). To rule out osmotic effects from additional levels of nutrients, we show that sorbitol at the same concentration (10 mM) did not rescue macrophage viability (Figure 3B). The delayed cell death of macrophages could also be seen when glucose or pyruvate were spiked 6 h post challenge (Figure 3C). Supplementing glucose delayed macrophage cell death in infections with *C. auris* isolates from all four clades (Figures 4A–4E). Taken together, these data show that, under these conditions, glycolysis is essential for viability of *C. auris*-infected macrophages.

Further consistent with increased glycolysis,[26,32–34] *C. auris* infection induced the expression of the macrophage *Glut1*

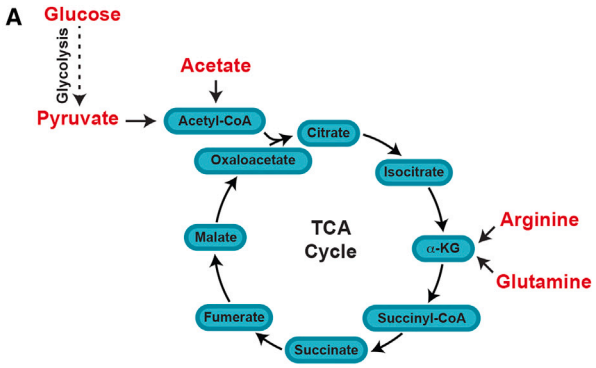

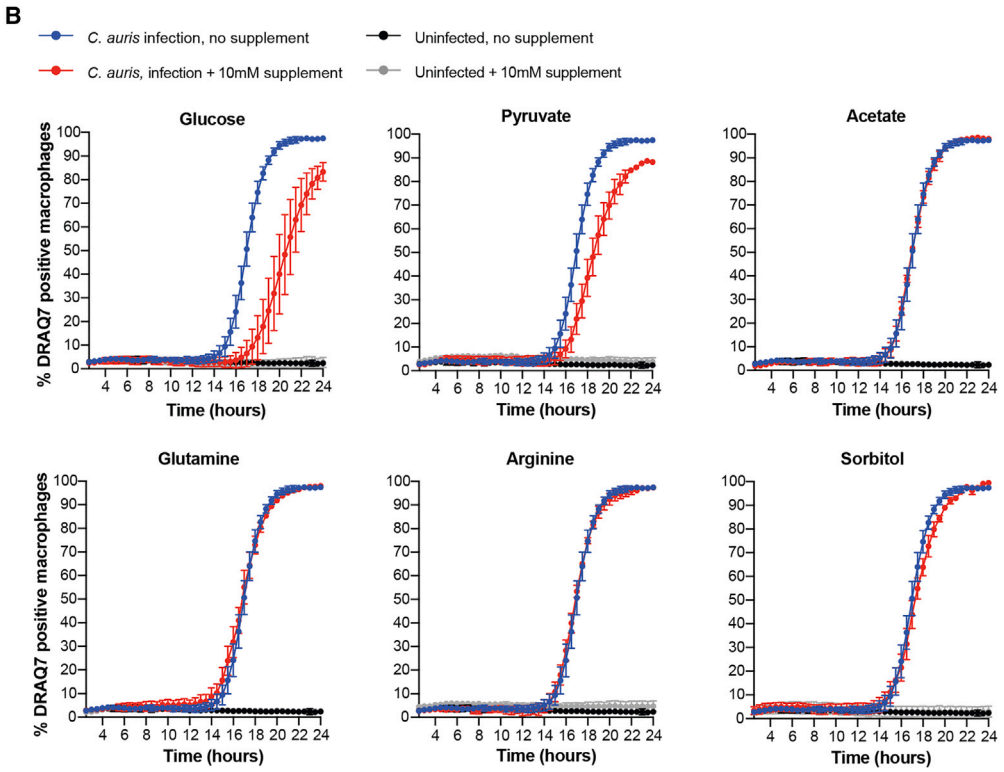

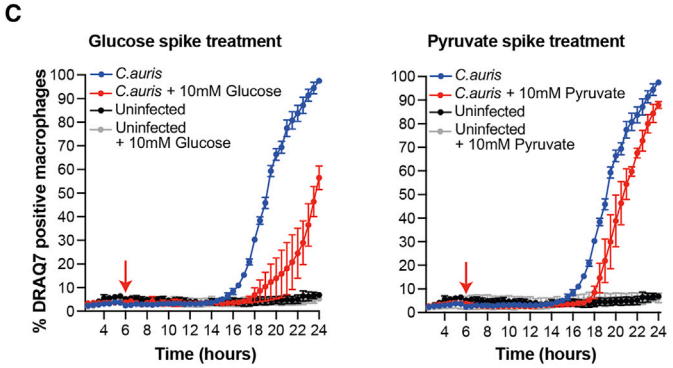

(legend on next page)

glucose transporter and the glycolytic enzymes *Hk2* and *Pfkbf3* (Figure 5A). *C. auris*-infected macrophages, but not *C. auris* cultured alone, also showed further signs of elevated glycolysis with heightened levels of lactate relative to uninfected controls (Figures 5B and S3A). Additionally, infected macrophages showed accelerated cell death in the presence of the antidiabetic drug metformin (Figure 5C). At the dose used, metformin was not toxic to uninfected macrophages (Figure 5C), and it did not affect the growth of *C. auris* (Figure S3B). Metformin's mode of action includes inhibition of mitochondrial complex I,[35,36] activation of AMP kinase,[37] and inhibition of the expression of glycolytic enzymes and glucose transporters.[38] Therefore, metformin could repress Warburg metabolism in macrophages similar to data in cancer cells.[39] As such, hyper-susceptibility to metformin is in line with *C. auris* triggering the Warburg effect and reliance on glycolysis in macrophages.

During Warburg metabolism, decreased mitochondrial respiration accompanies higher glycolysis, which could make glucose essential for macrophage survival. Indeed, depletion of glucose was observed as *C. auris* infection progressed (Figure 5D), and supplementation of glucose rescued *C. auris*-infected macrophages in a dose-dependent manner (Figure 5E). The survival of uninfected macrophages was not affected by glucose concentration (Figure 5E).

Increasing glucose concentration also led to increased growth of *C. auris* (Figure S3C), yet we observed less macrophage cell death under these conditions. These data argue against the hypothesis that *C. auris* is secreting toxic compounds/toxins that cause lytic cell death in macrophages, as these toxic metabolites would be expected to increase when yeast growth is more robust. Collectively, our results show that macrophages increase their glycolytic metabolism in response to *C. auris* but are unable to inhibit *C. auris* growth or kill the pathogen. We further show that *C. auris* kills macrophage by competing for their glucose supply.

C. auris metabolic capacity drives macrophage killing and is important for proliferation *in vivo*

To understand how *C. auris* utilizes its metabolic capacity during macrophage interactions, we created a mutant unable to perform glycolysis by deleting the gene encoding pyruvate kinase (*CDC19*). As expected, the *Δcdc19* mutant was unable to utilize glucose or fructose as a carbon source but grew on acetate, albeit more slowly than the wild type (Figures 6A and S4A). The *Δcdc19* mutant was unable to either escape or kill macrophages, even when acetate was supplemented to the medium to enable its growth (Figure 6B). Despite its limited capacity to utilize metabolites, we observed an increase in CFUs for the *Δcdc19* mutant within macrophages, showing that it can replicate although at a slower pace than the wild type (Figure S4B). This supports a key role of *C. auris* metabolic capacity in both immune egress and killing.

We next aimed to understand how *C. auris* regulates its metabolic capacity to kill macrophages and establish infection. For this, we created mutants in the transcriptional activators Tye7 and Gal4. Tye7 controls glycolysis in yeasts such as *C. albicans* and the distantly related model organism *S. cerevisiae*.[40,41] In *C. albicans*, Gal4 further contributes to glycolytic gene expression.[40] The *C. auris Δtye7* and *Δgal4* mutants grew in all carbon sources that we tested (fermentable and non-fermentable), even in the presence of the mitochondrial respiration inhibitor antimycin A that forces cells to use glycolysis (Figure 6C). A more detailed analyses in liquid medium confirmed that *Δgal4* displayed wild-type growth rates in glucose, which was consistent in two different strain backgrounds (470121 and B8441) (Figures S4C and S4D). This analysis revealed that *Δtye7* grew more slowly in log phase, with the average doubling time of almost 2 or 1.5 times the rate of the wild type for the 470121 and B8441 strains respectively (Figure S4D). However, *Δtye7* entered log phase normally and reached the same saturation as the wild-type strain at the conclusion of the time course (Figure S4C).

To test whether these transcription factors regulate glycolysis in *C. auris*, we first examined the expression of relevant glycolytic genes. Fungal cultures were grown as for the growth curves in Figure S4C, and samples taken at the 7-h time point when both wild type and mutants entered log phase and before differences in growth rate occur. The expression of glycolytic genes was reduced in *Δtye7* but not in *Δgal4* (Figure 6D). This suggests that Tye7 is a prominent transcriptional activator of glycolytic gene expression in *C. auris*. Consistent with this key metabolic role, *Δtye7* was slower than the wild type in triggering glucose depletion-dependent macrophage cell death (Figure 6E). This phenotype was consistent with independently created *Δtye7* mutants in two *C. auris* strain backgrounds: 470121 and B8441 (Figure 6E). In both backgrounds, the *Δgal4* mutant did not differ from the wild type (Figure 6E). Unfortunately, even after multiple attempts and using distinct transformation protocols, we were unsuccessful in creating a *Δtye7* complementation strain. This could be due to the documented difficulties in transforming *C. auris* and achieving marker integration at the desired locus.[42–44] As an alternative approach, we extended the macrophage infection assay to additional, independently isolated *Δtye7* mutant clones in both the 470121 and B8441 strains. All of the independent *Δtye7* mutants that we assayed showed a delay in triggering glucose depletion-dependent cell death of macrophages (Figures S6E and S4E). This phenotype is

Figure 3. *C. auris*-infected macrophages can be rescued by nutrient supplementation

(A) Central carbon metabolism (glycolysis and the TCA cycle). The nutrients indicated in red were supplemented to the medium in *C. auris*-macrophage infections.

(B) Macrophages (BMDMs) were challenged with *C. auris* 470121 as in Figure 2A (MOI 6). The indicated nutrients were added to standard macrophage infection medium, which contains 10 mM glucose. The blue graphs (labeled *C. auris*) are from infections performed in standard medium without supplementation of additional nutrients. All of the nutrient conditions were analyzed together in the same experiment but are plotted separately for clarity. As such, the standard medium (blue graph) is the same in all comparisons. Shown are the mean values and SEM for three independent experiments.

(C) Same as (B) but glucose or pyruvate were added at 6 h post infection (red arrow). The two nutrients were analyzed together in the same experiment but are plotted separately for clarity. As such, the standard medium (blue graph) and uninfected macrophage data are the same in all comparisons (these data are also the same as in Figure 2D). Shown here are the mean values and SEM for three independent experiments.

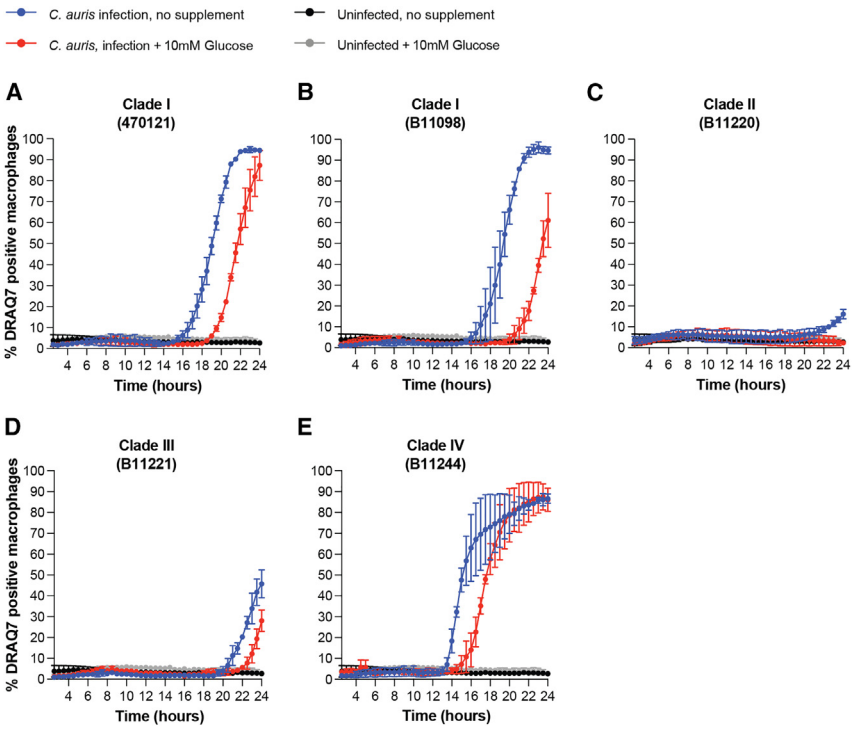

Figure 4. Rescue of macrophage viability by glucose is recapitulated across *C. auris* clades

(A–E) Macrophages (BMDMs) were challenged with the indicated *C. auris* isolates and imaged to quantify DRAQ7-positive macrophages (MOI 6). Shown are the mean and SEM for two independent experiments. At least 3,000 macrophages were imaged in each experiment for each of the experimental groups.

recapitulated in the *C. albicans Δ/Δtye7* mutant,[26] showing that Tye7 has a conserved role in enabling rapid glucose depletion and immune cell killing by *Candida* species *in vitro*.

Glycolytic metabolism was also important for establishing infection *in vivo*, as shown by reduced *C. auris* proliferation in kidneys of mice systemically infected with the *Δtye7* strain at day 2 after infection (Figure 6F). Given the slower growth of *Δtye7 in vitro* (Figure S4C), we extended the post-infection time to 5 days to address whether *Δtye7* simply needs more time to proliferate. However, CFU numbers for *Δtye7* did not increase at day 5 (Figure 6F, experiment 2). This shows that, even after prolonged times, the mutant is unable to grow in kidney tissues. By day 5, the wild-type CFUs decreased (Figure 6F), indicating that mice were clearing the infection. The host glucose transporter gene *Glut1* and the glycolytic enzymes *Hk2* and *Pfkbf3* were expressed at higher levels in kidneys infected with *Δtye7* compared with infections with wild-type *C. auris* (Figure 6G). This is consistent with an immunometabolic shift occurring in infected kidneys and suggests a stronger immune response to the mutant. We also observed that, unlike in response to *C. albicans*,[26] infection with our wild-type *C. auris* strain did not cause increased expression of these host glycolytic genes in infected over non-infected kidneys (Figure 6G). Collectively, these results show that *C. auris* glycolysis and the Tye7 activator are important for evading macrophages and for establishing infection in organs.

C. auris does not trigger robust NLRP3 inflammasome activation

Macrophage cell death alerts the host to infection and triggers inflammation.[45] In addition, disruption of macrophage glycolysis by infection activates the NLRP3 inflammasome in response to several pathogens.[28,46,47] In turn, the NLRP3 inflammasome triggers antimicrobial inflammation via maturation of the proinflammatory cytokines interleukin (IL)-1β and IL-18, as well as activating pyroptosis, a proinflammatory type of macrophage cell death that involves caspase-1/4/5/11-mediated cleavage and activation of the pore-forming protein gasdermin D (GSDMD).[48,49] Inspired by these studies, we tested whether *C. auris* incidentally triggers an immune response by causing macrophage metabolic stress and cell death.

By ELISA, we detected little secreted IL-1β in the supernatants of *C. auris*-infected macrophages at 1 h after challenge (Figure 7A). Secreted IL-1β increased at 10 h, but the concentration was low relative to the nigericin control and there was no additional increase at 16 h (Figure 7A). Measurements of LDH release on the same samples used for the ELISA confirmed that macrophages were dying at 16 h post infection (Figure 7B). Therefore, although macrophages were dying, the IL-1β response to *C. auris* was minimal. In view of the low IL-1β response, we next compared the inflammatory potential of *C. auris* with that of *C. albicans*, side by side, using the *C. albicans* isolate SC5314 that robustly activates the NLRP3 inflammasome.[50–53] *C. albicans* triggered high levels of IL-1β secretion (Figure 7C). Therefore, in our experimental system, macrophages activate strong inflammasome-dependent responses when infected with *C. albicans* but minimally with our *C. auris* isolate.

We also used biochemical approaches to directly test several further outputs of NLRP3 inflammasome activation. Western blot analyses of cellular lysates and supernatants largely confirmed the ELISA results, showing that *C. auris* fails to induce significant processing of IL-1β to its mature p17 form by the inflammasome-activated protease caspase-1 (Figures 7D and S5A). In comparison, *C. albicans* showed robust induction of IL-1β processing (Figures 7D and S5A). We also examined two further markers of NLRP3 inflammasome activation: caspase-1 autoproteolysis (p20) and caspase-1-mediated cleavage of GSDMD to its N-terminal pore-forming fragment (p30).[54–57] There was little evidence of caspase-1 or GSDMD cleavage upon *C. auris* infection (Figures 7D and S5A). Again, the control pathogen *C. albicans* induced both caspase-1 and GSDMD cleavage (Figures 7D and S5A). Finally, NLRP3 deficiency did not reduce *C. auris*-

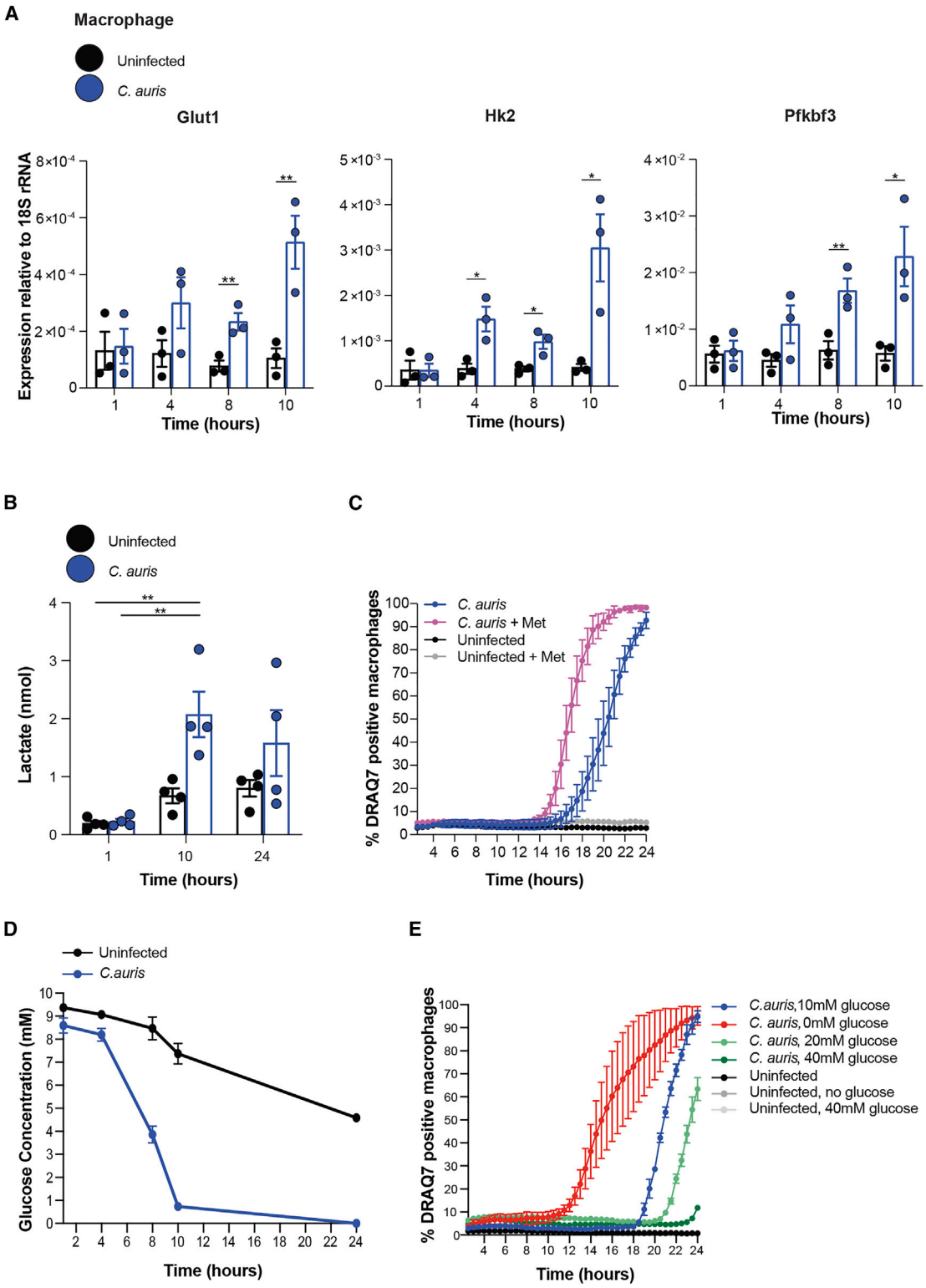

Figure 5. Immunometabolic adaptation of macrophages in response to *C. auris*

For all experiments, *C. auris* challenge was performed with BMDMs. The fungal strain was 470121 and the MOI was 6.

(A) Quantitative PCR analysis macrophage metabolic gene expression: the glucose importer *Glut1* and the glycolytic enzymes *Pfkfb3* and *Hk2* at 1, 4, 8, and 10 h after *C. auris* challenge. Gene expression was normalized to 18S rRNA. Shown are the mean values and SEM for three independent experiments, each analyzed in two technical replicates (one-tailed student t test, *p $\leq$ 0.05, **p $\leq$ 0.01). Only statistically significant comparisons are indicated.

(legend continued on next page)

induced macrophage cell death (Figure 7E), indicating that *C. auris* does not trigger NLRP3 inflammasome-dependent pyroptosis. Overall, our results suggest that our *C. auris* strain avoids substantial recognition by NLRP3, despite perturbing macrophage glycolysis and causing large-scale macrophage cell death.

To investigate whether other cell death pathways were involved in *C. auris*-induced macrophage death, we performed infections in an immortalized BMDM (iBMDM) cell line that is deficient for caspase-1, caspase-11, caspase-12, caspase-8, and Receptor-Interacting Protein Kinase 3 (RIPK3). As such, in this cell line, the cell death pathways of pyroptosis, necroptosis, and extrinsic apoptosis are abrogated. However, these deficiencies were unable to reduce *C. auris*-induced macrophage cell death (Figure 7F). The pan-caspase inhibitor quinoline-Val-Asp-difluorophenoxymethylketone (QVD) also did not cause a measurable delay in *C. auris*-induced macrophage cell death (Figure 7G). Last, we utilized a biochemical approach to test whether macrophage apoptosis is activated early in the infection, perhaps associated with *C. auris* escape from macrophages, but that may not be detected by our live-cell imaging assay that measures membrane permeabilization-dependent DRAQ7 staining. *C. auris* failed to induce significant processing of the apoptotic caspase 3 into the activation-associated fragments, p17 and p19, compared with the positive control stimulation (activation of intrinsic apoptosis with ABT-737 and S36845) (Figures 7H and S5B). Together, these results suggest that, under our experimental conditions, *C. auris*-induced macrophage cell death does not occur via these major cell death pathways.

DISCUSSION

Our study establishes how *C. auris* evades macrophages *in vitro* and shows that the mechanisms are grounded in metabolic regulation. We show that *C. auris* escapes from immune containment and kills macrophages by causing metabolic stress. *C. auris* escape and killing of macrophages are conserved in isolates from four different clades and are recapitulated between mouse and human primary macrophages. Our *C. auris* strain is able to disrupt host glycolysis and kill macrophages while avoiding robust activation of the NLRP3 inflammasome. This is in contrast with studies showing that disruption of macrophage glycolysis by *C. albicans*,[28] *Salmonella thyphimurium*,[47] and N-acetylglucosamine released from bacterial peptidoglycan[46] activates the NLRP3 inflammasome and antimicrobial inflammation. For other *Candida* species that, like *C. auris*, grow mostly in yeast morphology, the elicited immune response is mixed. For example *Candida glabrata* elicits a low cytokine response,[58] while *Candida guilliermondii* evokes an even stronger immunological response than *C. albicans*.[59] Therefore, it is interesting that our *C. auris* strain is able to utilize metabolic regulation to eliminate macrophages without the associated costs that come from activating strong NLRP3 inflammasome-dependent antimicrobial responses. We propose that this metabolic mechanism enables *C. auris* to survive and grow in infection niches. This proposition is supported by our data showing that deletion of the *C. auris* transcriptional activator *TYE7* reduces glycolytic gene expression, delays macrophage killing, and reduces fungal kidney burdens in the mouse bloodstream infection model. These findings also establish Tye7 as an important transcriptional regulator of *C. auris* metabolism and proliferation *in vivo*.

Our conclusion that *C. auris* egresses from macrophages and kills them contrasts with a recent study that showed no escape or macrophage damage by *C. auris*.[8] However, the authors only considered the first few hours after infection. By using our live-cell imaging platform, which allows for assessment of host-pathogen interactions over prolonged infection times, we demonstrate that escape does indeed occur, initiating at 8–10 h after challenge under our experimental conditions. We further show that macrophage damage also occurs, initiating at 16–18 h after challenge. *C. auris* escape differs from that of the related fungal pathogen *C. albicans*. *C. albicans* egresses from macrophages by growing invasively in hyphal form and activating two pore-forming proteins, fungal candidalysin and host gasdermin D (GSDMD), to damage macrophage membranes.[60–63] Our imaging data show that *C. auris* remains in yeast form as it escapes from macrophages, and we also demonstrate biochemically that it does not trigger the processing of GSDMD to its pore-forming fragment. Furthermore, *C. auris* does not encode the fungal toxin candidalysin in its genome.[64] Another yeast-locked pathogen, *C. glabrata*, also egresses from macrophages without hyphae, but data with human macrophages showed that this happens much later than what we see for *C. auris* (i.e., 3 days instead of 4–6 h) even though a similar multiplicity of infection was used between our study (MOI 6) and that of Sieder et al. (MOI 5).[58] Moreover, the escape of *C. glabrata* is associated with macrophage lysis due to high fungal loads after 3 days of growth.[58] This also contrasts with *C. auris*, as our data suggest that its escape is not associated with overt macrophage lysis: we saw no increase in LDH release or clear increases in DRAQ7 staining over uninfected controls until past 18 h after infection (with an MOI of 3; Figures 1C and 2A). This is despite the fact that the escape of *C. auris* starts well before 18 h and is seen at 8 h after infection (Figures 1A and 1B).

Our data support a critical role for fungal metabolic capacity in *C. auris* immune escape, since the pyruvate kinase mutant *Δcdc19* is unable to escape from macrophages or kill them

(B) Production of lactate for *C. auris*-infected and uninfected BMDMs 1, 10, and 24 h after challenge. Shown are the means and SEM from four independent experiments (two-way ANOVA Bonferroni's multiple comparison test compared the 10- and 24-h with the 1-h infection conditions; $^{**}p \leq 0.01$). Only statistically significant comparisons are indicated.
(C) Macrophages were pre-treated with 5 mM metformin for 24 h and then switched to fresh medium with and without metformin, followed by challenge with *C. auris*. Uninfected macrophage controls were treated the same. Shown are the mean values and SEM for three independent experiments.
(D) Reduction in glucose levels over the time course of *C. auris*-macrophage infection. Shown are the mean values and SEM for three independent experiments.
(E) Macrophage cell death during *C. auris* infection with increasing glucose concentrations. The control condition (blue) contains 10 mM glucose. Shown are the mean values and SEM for three independent experiments.

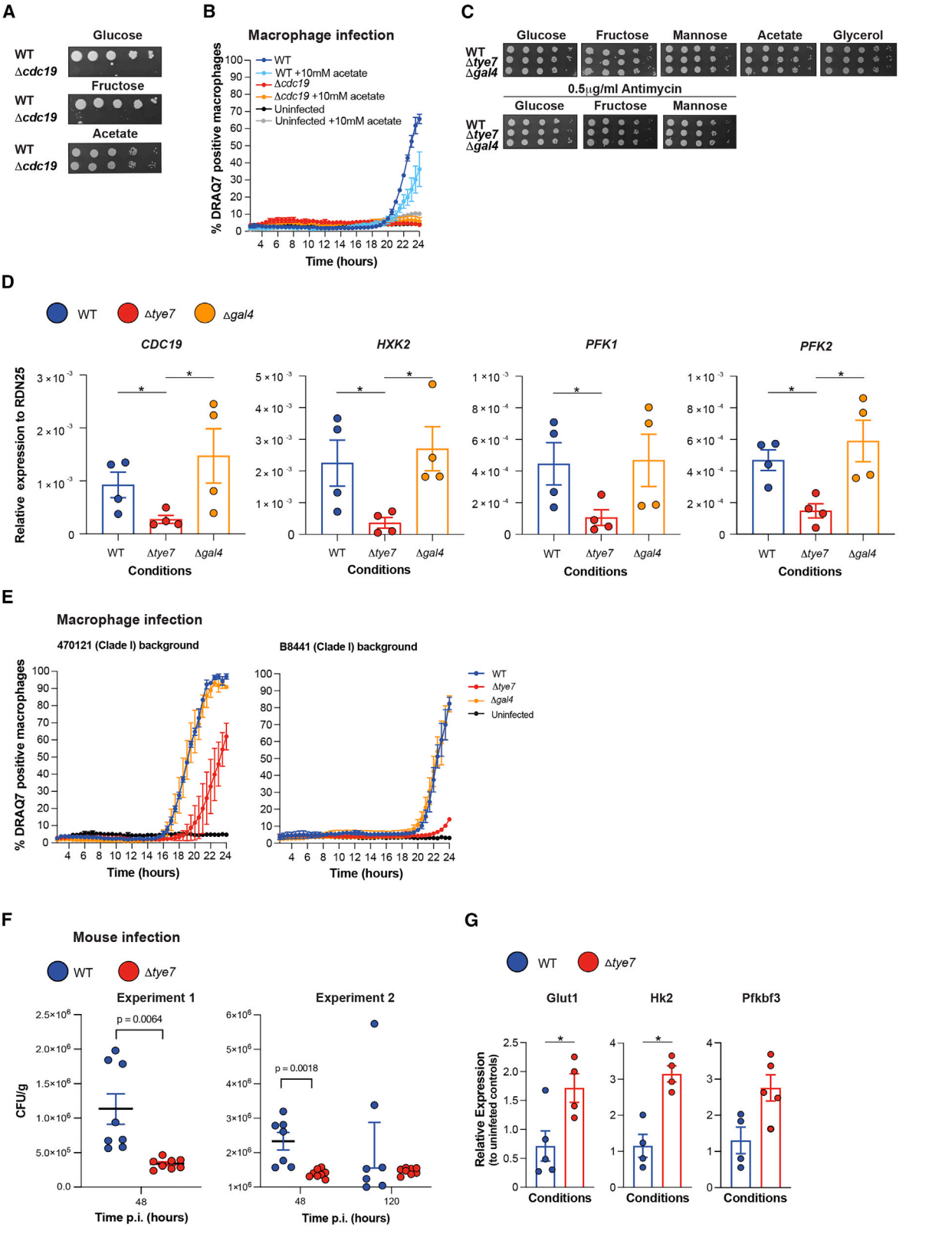

(legend on next page)

even when acetate is supplemented to support its growth (Figure 6). Metabolic capacity enables *C. auris* proliferation in macrophages, which could serve to increase pathogen loads to a sufficient degree to trigger non-lytic escape. Indeed, although the *Δcdc19* can replicate in macrophages, it does so to a significantly lower degree than the wild-type strain (Figure S4B).

On the host side, we present evidence that *C. auris*-infected macrophages undergo immunometabolic shifts to increase their glycolytic metabolism. Increased macrophage glycolysis is a conserved response to bacterial and fungal pathogens, as well as microbial ligands.[16,18,20,26,65] *C. auris*-infected PBMCs did not display transcriptional signatures of increased glycolysis, and it was therefore suggested that this metabolic response of immune phagocytes might be different with *C. auris*.[8] Our data challenge this conclusion. We further show that glycolysis is critically important for *C. auris*-infected macrophages, as macrophages were rescued from *C. auris*-induced cell death by glucose and pyruvate (the terminal metabolite of glycolysis) but not by acetate, glutamine, or arginine. Differences in experimental conditions, including distinct *C. auris* isolates and immune cell types (PBMCs versus BMDMs), could explain these contrasting conclusions.

Macrophage killing by *C. auris* depends on their reliance on glucose, which is a consequence of their immunometabolic shift. Our animal infection study with the *Δtye7* mutant shows that regulation of *C. auris* glycolytic metabolism is important in animal infections, and it also supports a role for host glycolysis, as we detected an upregulation of host glycolytic gene expression in *Δtye7*-infected kidneys. It was curious that infection with the wild-type strain did not cause upregulation of these same host glycolytic genes, in contrast with our results with *C. albicans* in a similar infection context.[26] A lower virulence of *C. auris* relative to *C. albicans* in the bloodstream mouse model[8] could explain the different metabolic response. However, this explanation does not fit with the fact that *Δtye7* shows a lower load in mouse kidneys than wild-type *C. auris*, yet the host glycolytic pathway is induced. It will be important to test many more diverse *C. auris* isolates to precisely understand the host metabolic response *in vivo*.

We found a difference between *C. auris* and previously studied pathogens with respect to the roles of macrophage glycolysis in antimicrobial responses. Increased glycolysis contributes to antifungal immune responses and cytokine production by macrophages and monocytes in response to *C. albicans* and *Aspergillus fumigatus*[18,20] and also in response to several bacterial pathogens.[16,66,67] However, we show that these functions are not recapitulated with our strain of *C. auris*. We detected little IL-1β secretion by *C. auris*-infected macrophages and minimal signs of processing of this cytokine to its active form by the NLRP3 inflammasome. Our conclusion is supported by a study published while our manuscript was in preparation, which also showed low IL-1β secretion by *C. auris*-infected mouse macrophages (BMDMs).[6] In contrast, a recent report with human PBMCs concluded that *C. auris*-induced cytokine responses were more potent relative to *C. albicans*.[8] Differences in cytokine secretion could reflect the use of distinct *C. auris* isolates and immune cell types.[6] Wang et al. attributed low cytokine responses to reduced recognition and phagocytosis of *C. auris* by macrophages, but we see effective phagocytosis. Our data instead suggest that our *C. auris* strain is not competent to activate the NLRP3 inflammasome. Specifically, we could not detect substantial activation of any of the known outputs of NLRP3 inflammasome, as there was little processing of IL-1β, caspase-1, or GSDMD and no activation of pyroptosis in *C. auris*-infected macrophages. Our data also suggest a lack of activation of apoptosis by *C. auris* and no role for either apoptosis or necroptosis in the cell death of *C. auris*-infected macrophages.

NLRP3 activation usually requires two signals. Based on work with *C. albicans*, signal 1 is provided by recognition of fungal cell wall components by macrophage receptors, while signal 2 is provided by rupture of the phagosomal membrane by invasive hyphal growth.[50,51,68] Hiding of β-glucan by *C. auris* mannan has been proposed to prevent immune recognition,[6] and this could reduce signal 1. However, this is not a likely explanation in our hands since, in our experiments that assess inflammasome outputs (Figure 7), pre-treatment of macrophages with lipopolysaccharide (LPS)provides signal 1. Therefore, it is possible that signal 2 is not robust with our *C. auris* strain. It will be exciting to dissect how *C. auris* hides from the NLRP3 inflammasome.

In conclusion, our findings establish important mechanisms of macrophage evasion by *C. auris* involving metabolic adaptations

Figure 6. Roles of *C. auris* metabolic capacity in macrophage killing and proliferation *in vivo*

(A) Spot assays of the *C. auris* pyruvate kinase mutant *Δcdc19* relative to its isogenic wild type (strain B8441) with glucose, fructose, or acetate as the carbon source. Growth was assessed after 3 days at 30°C.

(B) Macrophages (BMDMs) were challenged with *C. auris* wild type (strain B8441) or its isogenic *Δcdc19* strain (MOI 6). DRAQ7-positive macrophages were quantified using live-cell imaging. Shown are the mean values and SEM for three independent experiments.

(C) Spot assays for *C. auris* wild type, *Δtye7*, and *Δgal4* mutants. Cultures were plated on the indicated plates and photographed after 3 days of growth at 30°C.

(D) Yeast cultures were grown as in Figure S4B and samples taken after 7 h, when both wild type and mutants enter log phase. The expression of the indicated glycolysis genes was assayed using qPCR and normalized to *RDN25*. Shown are the means and SEM of four independent experiments. *$p \leq 0.05$ (Kruskal-Wallis non-parametric test and Dunn's multi-comparison test).

(E) Macrophages (BMDMs) were challenged with *C. auris* wild type, *Δtye7*, and *Δgal4* in either the 470121 or the B8441 strain background, and DRAQ7-positive macrophages were quantified using live-cell imaging (MOI 6). Shown are the mean values and SEM for three independent experiments.

(F) Mice were infected with *C. auris* wild type or *Δtye7* (470121 background) and kidney CFUs determined after 48 h. Two different experiments were performed. In the second experiment, a further time point of 120 h was sampled. Statistical analysis was performed using the Kruskal-Wallis non-parametric test and Dunn's multi-comparison test.

(G) Experimental conditions were as in (F) and RNA samples taken at 48 h. The expression of the indicated mouse glycolysis genes was assayed using qPCR and normalized to *18S RNA* and uninfected controls. Shown are the means and SEM of four or five independent individuals (one-way ANOVA Bonferroni's multiple comparison test, *$p \leq 0.05$). Only statistically significant comparisons are indicated.

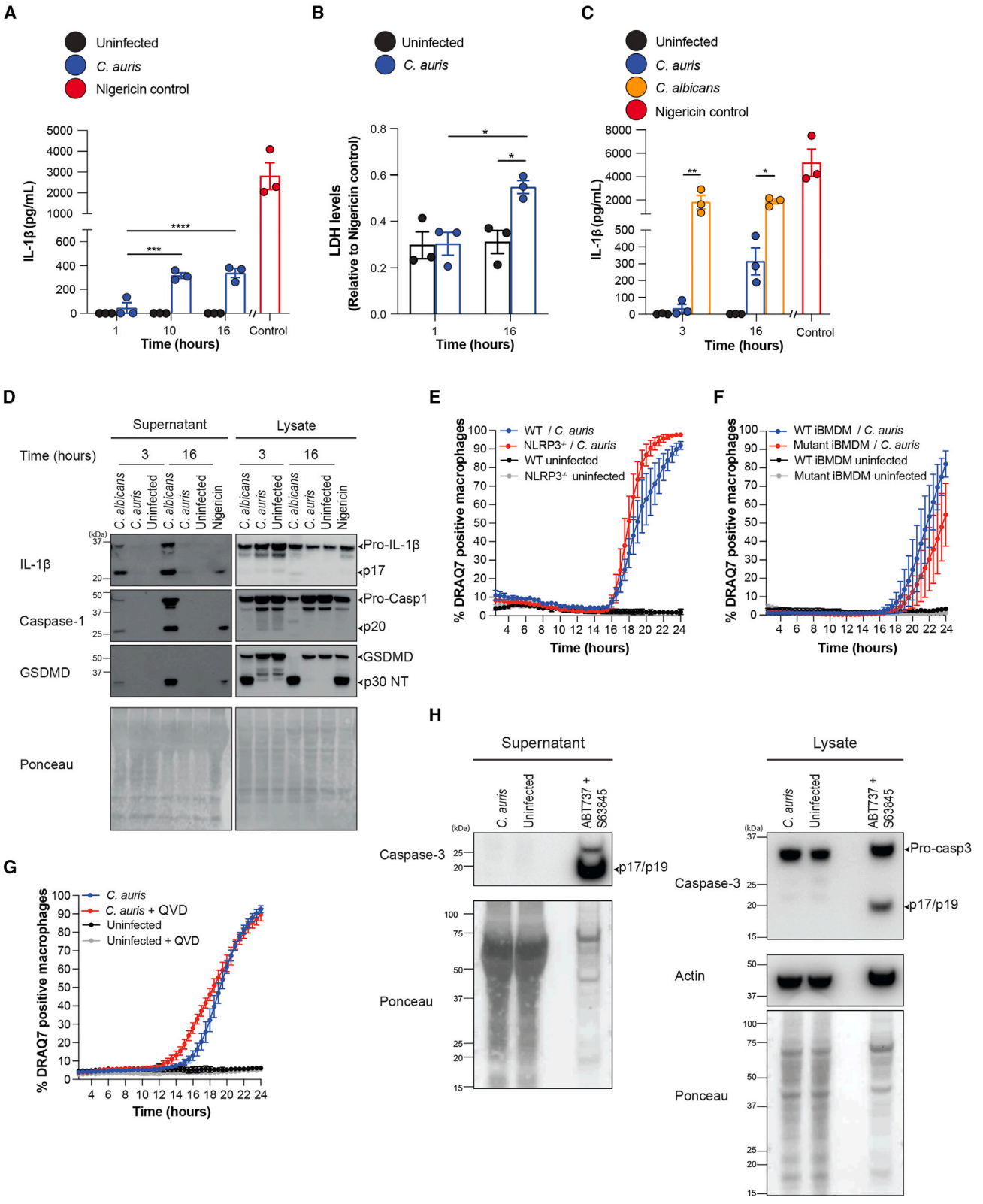

(legend on next page)

that promote egress from the immune phagocytes and creation of a nutrient-poor infection niche in which macrophages cannot survive. Unexpectedly, macrophage cell death and disruption of host glycolysis by our *C. auris* isolate did not activate the NLRP3 inflammasome in a significant manner. Thereby, macrophage IL-1β responses remained low. This could reduce the recruitment of other immune cells into infection sites.

Limitations of the study

Our data show that the escape of *C. auris* from macrophages and macrophage killing by glucose depletion are conserved mechanisms across a range of isolates belonging to four genetic clades. However, our cytokine and inflammasome studies were limited to one clade I isolate. Given the contrasting conclusions on IL-1β responses to *C. auris* from studies to date, future work should address inflammasome and cytokine responses to a broad range of isolates. This will allow us to understand more broadly how *C. auris* evades macrophages and activates or evades proinflammatory activation.

We also need to precisely understand the regulation of host and *C. auris* metabolism *in vivo*, in the complex infection environment within tissues and organs. Understanding how knowledge from animal infections translates to human patients will also be crucial. As we have previously proposed,[26] the formation of zones of concentrated fungal proliferation in tissues and organs could create microenvironments where lower glucose concentrations inhibit the clearance of pathogens by immune cells (macrophages, monocytes, and neutrophils). Indeed, neutrophils also need glucose for antifungal responses, as has been demonstrated for *C. albicans* in a recent study.[69] *C. auris* is poorly killed by neutrophils,[70] and it will be interesting to determine whether metabolic mechanisms and glucose deprivation play a role in its neutrophil evasion.

The evidence that survival of patients with infections and sepsis is assisted by metabolic regulation is accumulating,[9,15,71] and our study provides some of the first findings on the interplay of host and pathogen metabolism in *C. auris* infections. Given that *C. auris* can be resistant to all current classes of antifungal drugs, it is important to find alternative treatment strategies. Deeper understanding of metabolism in *C. auris* infections will contribute to this goal.

STAR★METHODS

Detailed methods are provided in the online version of this paper and include the following:

- KEY RESOURCES TABLE
- RESOURCE AVAILABILITY
  - Lead contact
  - Materials availability
  - Data and code availability
- EXPERIMENTAL MODELS
  - *Candida* strains and media
  - Strain construction
  - Isolation of murine bone marrow derived macrophages (BMDMs) and human monocyte-derived macrophages (hMDMs)
- METHOD DETAILS
  - Live cell imaging
  - Collection of supernatants and lysates for IL-1® ELISA, lactate dehydrogenase (LDH) and western blot assays
  - IL-1β ELISA
  - LDH assay
  - Western blot
  - Lactate assay
  - Quantification of glucose
  - Colony forming unit (CFU) measurements
  - pH measurements of media
  - Growth curves

Figure 7. Macrophages fail to robustly activate the NLRP3 inflammasome in response to *C. auris*

(A) ELISA of IL-1β release in response to *C. auris* infection of BMDMs. Macrophages were primed with 50 ng/mL lipopolysaccharide (LPS) for 3 h, followed by challenge with *C. auris* (strain 470121) for 1, 10, and 16 h. The NLRP3 activator nigericin was the positive control and uninfected macrophages the negative control. Shown are the mean values and SEM for three independent experiments (two-way ANOVA Bonferroni's multiple comparison test compared the 10- and 16-h infection condition with the 1-h time point; ***$p \leq 0.001$, ****$p \leq 0.0001$).

(B) LDH release for *C. auris*-infected and uninfected macrophages at 1 and 16 h after challenge. The assay was performed on the supernatants from (A). Values are expressed relative to the nigericin control. Shown are the mean values and SEM from three independent experiments (two-way ANOVA Bonferroni's multiple comparison test was performed; *$p \leq 0.05$).

(C) IL-1β ELISA was done as in (A). Macrophages were primed with LPS and challenged with *C. auris* (strain 470121), *C. albicans* (strain SC5314), or uninfected for 3 and 16 h. Shown are the mean values and SEM for three independent experiments (two-way ANOVA Bonferroni's multiple comparison test; *$p \leq 0.05$, **$p \leq 0.01$).

(D) Immunoblot of supernatants and lysates from the samples in (C). *C. albicans* and 10 μM nigericin were used as positive controls and Ponceau staining as the loading control. The mature (active) IL-1β is the p17 fragment, for caspase it is the p20 fragment, and p30 for Gasdermin D (GSDMD). A representative experiment is shown. Uncropped immunoblots for three independent experiments are shown in Figure S5A.

(E) BMDMs from wild type or *Nlrp3*$^{-/-}$ mutant mice were infected with *C. auris* 470121 (MOI 6) and DRAQ7-positive macrophages quantified using live-cell imaging. Shown are the means and SEM for three independent experiments.

(F) As in (E), but comparing immortalized BMDMs (iBMDM) wild type with mutants for caspase-1, caspase-11, caspase-12, caspase-8, and Receptor-Interacting Protein Kinase 3 (RIPK3). Shown are the means and SEM for three independent experiments. WT, wild type.

(G) Wild type BMDMs were challenged as in (E), treated with or without pan-caspase inhibitor QVD (10 μM). Shown are the mean and SEM for three independent experiments.

(H) Immunoblot analysis of supernatants and lysates from macrophages challenged with *C. auris* 470121 for 3 h. The caspase 3 activator ABT737 + S63845 was used to activate intrinsic apoptosis as a positive control and uninfected macrophages as a negative control. Ponceau staining or actin were used as loading controls. The mature (active) Caspase3 is the p17/p19 fragment. A representative experiment is shown. Uncropped immunoblots for three independent experiments are shown in Figure S5B.

- Phagocytosis determinations
- Quantitative PCR analysis (qPCR)
- Animal infections

● QUANTIFICATION AND STATISTICAL ANALYSIS

SUPPLEMENTAL INFORMATION

Supplemental information can be found online at https://doi.org/10.1016/j.celrep.2023.112522.

ACKNOWLEDGMENTS

We thank Sarah Kidd (Australian Mycology Reference Centre) and Sharon Chen for the *C. auris* strain 470121 and Anastasia Litvintseva from the CDC for their panel of *C. auris* strains. We further thank James Vince and Seth Masters (Walter and Eliza Hall Institute) for providing *Nlrp3*$^{-/-}$ macrophages; Marco Herold, Yexuan Deng, and Marcel Doerflinger for the iBMDM macrophages inactivated for cell death pathways; Gareth Howells for assistance with calculating doubling times; and the Monash MicroImaging Facility (MMI) for expert support with microscopy. This work was supported by grants from the Australian National Health and Medical Research Council (NHMRC) (APP1158678 to A.T., APP2002520 to A. T. and R.B.-A., and APP1181089 to K.E.L.). R.B.-A. is further supported by Israel Science Foundation grant 442/18 and Ministry of Science and Technology grant 88555. C.S. is supported by a fellowship from the Monash-Warwick Alliance AMR Training Program. A.T. and K.E.L. are Future Fellows of the Australian Research Council (FT190100733 to A.T. and FT19010266 to K.E.L.).

AUTHOR CONTRIBUTIONS

H.W., C.S., R.B.-A., and A.T. designed the study. H.W., C.S., T.M.D., I.T., T.L.L., D.S.S., D.S., N.M., F.A.B.O., and M.S. performed the experiments. H.W., C.S., D.S.S., D.S., and N.M. analyzed the data. R.B.-A., K.E.L., and A.T. provided advice on experimental approach and data interpretation. A.T., K.E.L., and R.B.-A. obtained funding. A.T. wrote the manuscript with contributions from H.W. and editorial contributions from all authors.

DECLARATION OF INTERESTS

D.S. received honoraria and/or sat on advisory boards of Gilead, MSD, GSK, Pfizer, and Astra Zeneca. R.B.-M. served on advisory boards for Pfizer and Merck and received compensation from Teva and Gilead for lectures.

INCLUSION AND DIVERSITY

One or more of the authors of this paper self-identifies as an underrepresented ethnic minority in their field of research or within their geographical location. One or more of the authors of this paper self-identifies as a member of the LGBTQIA+ community. One or more of the authors of this paper self-identifies as living with a disability.

Received: August 16, 2022
Revised: March 28, 2023
Accepted: May 1, 2023
Published: May 18, 2023

REFERENCES

1. Jeffery-Smith, A., Taori, S.K., Schelenz, S., Jeffery, K., Johnson, E.M., Borman, A., Candida auris Incident Management Team; Manuel, R., and Brown, C.S. (2018). Candida auris: a review of the literature. Clin. Microbiol. Rev. *31*, e00029-17. https://doi.org/10.1128/cmr.00029-17.
2. Nett, J.E. (2019). Candida auris: an emerging pathogen "incognito. PLoS Pathog. *15*, e1007638. https://doi.org/10.1371/journal.ppat.1007638.
3. Hanson, B.M., Dinh, A.Q., Tran, T.T., Arenas, S., Pronty, D., Gershengorn, H.B., Ferreira, T., Arias, C.A., and Shukla, B.S. (2021). Candida auris invasive infections during a COVID-19 case surge. Antimicrob. Agents Chemother. *65*, e0114621. https://doi.org/10.1128/aac.01146-21.
4. Jacobs, S.E., Jacobs, J.L., Dennis, E.K., Taimur, S., Rana, M., Patel, D., Gitman, M., Patel, G., Schaefer, S., Iyer, K., et al. (2022). Candida auris pan-drug-resistant to four classes of antifungal agents. Antimicrob. Agents Chemother. *66*, e0005322. https://doi.org/10.1128/aac.00053-22.
5. Drummond, R.A., Gaffen, S.L., Hise, A.G., and Brown, G.D. (2014). Innate defense against fungal pathogens. Cold Spring Harb. Perspect. Med. *5*, a019620. https://doi.org/10.1101/cshperspect.a019620.
6. Wang, Y., Zou, Y., Chen, X., Li, H., Yin, Z., Zhang, B., Xu, Y., Zhang, Y., Zhang, R., Huang, X., et al. (2022). Innate immune responses against the fungal pathogen Candida auris. Nat. Commun. *13*, 3553. https://doi.org/10.1038/s41467-022-31201-x.
7. Horton, M.V., Johnson, C.J., Zarnowski, R., Andes, B.D., Schoen, T.J., Kernien, J.F., Lowman, D., Kruppa, M.D., Ma, Z., Williams, D.L., et al. (2021). Candida auris cell wall mannosylation contributes to neutrophil evasion through pathways divergent from Candida albicans and Candida glabrata. mSphere *6*, e0040621. https://doi.org/10.1128/mSphere.00406-21.
8. Bruno, M., Kersten, S., Bain, J.M., Jaeger, M., Rosati, D., Kruppa, M.D., Lowman, D.W., Rice, P.J., Graves, B., Ma, Z., et al. (2020). Transcriptional and functional insights into the host immune response against the emerging fungal pathogen Candida auris. Nat. Microbiol. *5*, 1516–1531. https://doi.org/10.1038/s41564-020-0780-3.
9. Traven, A., and Naderer, T. (2019). Central metabolic interactions of immune cells and microbes: prospects for defeating infections. EMBO Rep. *20*, e47995. https://doi.org/10.15252/embr.201947995.
10. Russell, D.G., Huang, L., and VanderVen, B.C. (2019). Immunometabolism at the interface between macrophages and pathogens. Nat. Rev. Immunol. *19*, 291–304. https://doi.org/10.1038/s41577-019-0124-9.
11. Troha, K., and Ayres, J.S. (2020). Metabolic adaptations to infections at the organismal level. Trends Immunol. *41*, 113–125. https://doi.org/10.1016/j.it.2019.12.001.
12. Weerasinghe, H., and Traven, A. (2020). Immunometabolism in fungal infections: the need to eat to compete. Curr. Opin. Microbiol. *58*, 32–40. https://doi.org/10.1016/j.mib.2020.07.001.
13. Rosenberg, G., Riquelme, S., Prince, A., and Avraham, R. (2022). Immunometabolic crosstalk during bacterial infection. Nat. Microbiol. *7*, 497–507. https://doi.org/10.1038/s41564-022-01080-5.
14. De Waele, E., Malbrain, M.L.N.G., and Spapen, H. (2020). Nutrition in sepsis: a bench-to-bedside review. Nutrients *12*, 395. https://doi.org/10.3390/nu12020395.
15. Van Wyngene, L., Vandewalle, J., and Libert, C. (2018). Reprogramming of basic metabolic pathways in microbial sepsis: therapeutic targets at last? EMBO Mol. Med. *10*, e8712. https://doi.org/10.15252/emmm.201708712.
16. Tannahill, G.M., Curtis, A.M., Adamik, J., Palsson-McDermott, E.M., McGettrick, A.F., Goel, G., Frezza, C., Bernard, N.J., Kelly, B., Foley, N.H., et al. (2013). Succinate is an inflammatory signal that induces IL-1β through HIF-1α. Nature *496*, 238–242. https://doi.org/10.1038/nature11986.
17. Cheng, S.C., Scicluna, B.P., Arts, R.J.W., Gresnigt, M.S., Lachmandas, E., Giamarellos-Bourboulis, E.J., Kox, M., Manjeri, G.R., Wagenaars, J.A.L., Cremer, O.L., et al. (2016). Broad defects in the energy metabolism of leukocytes underlie immunoparalysis in sepsis. Nat. Immunol. *17*, 406–413. https://doi.org/10.1038/ni.3398.
18. Domínguez-Andrés, J., Arts, R.J.W., Ter Horst, R., Gresnigt, M.S., Smeekens, S.P., Ratter, J.M., Lachmandas, E., Boutens, L., van de Veerdonk, F.L., Joosten, L.A.B., et al. (2017). Rewiring monocyte glucose metabolism via C-type lectin signaling protects against disseminated candidiasis. PLoS Pathog. *13*, e1006632. https://doi.org/10.1371/journal.ppat.1006632.
19. Lachmandas, E., Boutens, L., Ratter, J.M., Hijmans, A., Hooiveld, G.J., Joosten, L.A.B., Rodenburg, R.J., Fransen, J.A.M., Houtkooper, R.H.,

van Crevel, R., et al. (2016). Microbial stimulation of different Toll-like receptor signalling pathways induces diverse metabolic programmes in human monocytes. Nat. Microbiol. *2*, 16246. https://doi.org/10.1038/nmicrobiol.2016.246.

20. Gonçalves, S.M., Duarte-Oliveira, C., Campos, C.F., Aimanianda, V., Ter Horst, R., Leite, L., Mercier, T., Pereira, P., Fernández-García, M., Antunes, D., et al. (2020). Phagosomal removal of fungal melanin reprograms macrophage metabolism to promote antifungal immunity. Nat. Commun. *11*, 2282. https://doi.org/10.1038/s41467-020-16120-z.

21. Michelucci, A., Cordes, T., Ghelfi, J., Pailot, A., Reiling, N., Goldmann, O., Binz, T., Wegner, A., Tallam, A., Rausell, A., et al. (2013). Immune-responsive gene 1 protein links metabolism to immunity by catalyzing itaconic acid production. Proc. Natl. Acad. Sci. USA *110*, 7820–7825. https://doi.org/10.1073/pnas.1218599110.

22. Mills, E.L., Kelly, B., Logan, A., Costa, A.S.H., Varma, M., Bryant, C.E., Tourlomousis, P., Däbritz, J.H.M., Gottlieb, E., Latorre, I., et al. (2016). Succinate dehydrogenase supports metabolic repurposing of mitochondria to drive inflammatory macrophages. Cell *167*, 457–470.e13. https://doi.org/10.1016/j.cell.2016.08.064.

23. Jha, A.K., Huang, S.C.C., Sergushichev, A., Lampropoulou, V., Ivanova, Y., Loginicheva, E., Chmielewski, K., Stewart, K.M., Ashall, J., Everts, B., et al. (2015). Network integration of parallel metabolic and transcriptional data reveals metabolic modules that regulate macrophage polarization. Immunity *42*, 419–430. https://doi.org/10.1016/j.immuni.2015.02.005.

24. Tomlinson, K.L., Lung, T.W.F., Dach, F., Annavajhala, M.K., Gabryszewski, S.J., Groves, R.A., Drikic, M., Francoeur, N.J., Sridhar, S.H., Smith, M.L., et al. (2021). Staphylococcus aureus induces an itaconate-dominated immunometabolic response that drives biofilm formation. Nat. Commun. *12*, 1399. https://doi.org/10.1038/s41467-021-21718-y.

25. Riquelme, S.A., Liimatta, K., Wong Fok Lung, T., Fields, B., Ahn, D., Chen, D., Lozano, C., Sáenz, Y., Uhlemann, A.C., Kahl, B.C., et al. (2020). Pseudomonas aeruginosa utilizes host-derived itaconate to redirect its metabolism to promote biofilm formation. Cell Metab. *31*, 1091–1106.e6. https://doi.org/10.1016/j.cmet.2020.04.017.

26. Tucey, T.M., Verma, J., Harrison, P.F., Snelgrove, S.L., Lo, T.L., Scherer, A.K., Barugahare, A.A., Powell, D.R., Wheeler, R.T., Hickey, M.J., et al. (2018). Glucose homeostasis is important for immune cell viability during Candida challenge and host survival of systemic fungal infection. Cell Metab. *27*, 988–1006.e7. https://doi.org/10.1016/j.cmet.2018.03.019.

27. Wickersham, M., Wachtel, S., Wong Fok Lung, T., Soong, G., Jacquet, R., Richardson, A., Parker, D., and Prince, A. (2017). Metabolic stress drives keratinocyte defenses against Staphylococcus aureus infection. Cell Rep. *18*, 2742–2751. https://doi.org/10.1016/j.celrep.2017.02.055.

28. Tucey, T.M., Verma, J., Olivier, F.A.B., Lo, T.L., Robertson, A.A.B., Naderer, T., and Traven, A. (2020). Metabolic competition between host and pathogen dictates inflammasome responses to fungal infection. PLoS Pathog. *16*, e1008695. https://doi.org/10.1371/journal.ppat.1008695.

29. Simm, C., Weerasinghe, H., Thomas, D.R., Harrison, P.F., Newton, H.J., Beilharz, T.H., and Traven, A. (2022). Disruption of iron homeostasis and mitochondrial metabolism are promising targets to inhibit Candida auris. Microbiol. Spectr. *10*, e0010022. https://doi.org/10.1128/spectrum.00100-22.

30. Tucey, T.M., Verma-Gaur, J., Nguyen, J., Hewitt, V.L., Lo, T.L., Shingu-Vazquez, M., Robertson, A.A.B., Hill, J.R., Pettolino, F.A., Beddoe, T., et al. (2016). The endoplasmic reticulum-mitochondrion tether ERMES orchestrates fungal immune evasion, illuminating inflammasome responses to hyphal signals. mSphere *1*, e00074-16. https://doi.org/10.1128/mSphere.00074-16.

31. Lockhart, S.R., Etienne, K.A., Vallabhaneni, S., Farooqi, J., Chowdhary, A., Govender, N.P., Colombo, A.L., Calvo, B., Cuomo, C.A., Desjardins, C.A., et al. (2017). Simultaneous emergence of multidrug-resistant Candida auris on 3 continents confirmed by whole-genome sequencing and epidemiological analyses. Clin. Infect. Dis. *64*, 134–140. https://doi.org/10.1093/cid/ciw691.

32. Freemerman, A.J., Johnson, A.R., Sacks, G.N., Milner, J.J., Kirk, E.L., Troester, M.A., Macintyre, A.N., Goraksha-Hicks, P., Rathmell, J.C., and Makowski, L. (2014). Metabolic reprogramming of macrophages: glucose transporter 1 (GLUT1)-mediated glucose metabolism drives a proinflammatory phenotype. J. Biol. Chem. *289*, 7884–7896. https://doi.org/10.1074/jbc.M113.522037.

33. Rodríguez-Prados, J.C., Través, P.G., Cuenca, J., Rico, D., Aragonés, J., Martín-Sanz, P., Cascante, M., and Boscá, L. (2010). Substrate fate in activated macrophages: a comparison between innate, classic, and alternative activation. J. Immunol. *185*, 605–614. https://doi.org/10.4049/jimmunol.0901698.

34. Kelly, B., and O'Neill, L.A.J. (2015). Metabolic reprogramming in macrophages and dendritic cells in innate immunity. Cell Res. *25*, 771–784. https://doi.org/10.1038/cr.2015.68.

35. Owen, M.R., Doran, E., and Halestrap, A.P. (2000). Evidence that metformin exerts its anti-diabetic effects through inhibition of complex 1 of the mitochondrial respiratory chain. Biochem. J. *348*, 607–614.

36. Kelly, B., Tannahill, G.M., Murphy, M.P., and O'Neill, L.A.J. (2015). Metformin inhibits the production of reactive oxygen species from NADH:ubiquinone oxidoreductase to limit induction of interleukin-1β (IL-1β) and boosts interleukin-10 (IL-10) in lipopolysaccharide (LPS)-activated macrophages. J. Biol. Chem. *290*, 20348–20359. https://doi.org/10.1074/jbc.M115.662114.

37. Zhou, G., Myers, R., Li, Y., Chen, Y., Shen, X., Fenyk-Melody, J., Wu, M., Ventre, J., Doebber, T., Fujii, N., et al. (2001). Role of AMP-activated protein kinase in mechanism of metformin action. J. Clin. Invest. *108*, 1167–1174. https://doi.org/10.1172/jci13505.

38. Wahdan-Alaswad, R.S., Edgerton, S.M., Salem, H.S., and Thor, A.D. (2018). Metformin targets glucose metabolism in triple negative breast cancer. J. Oncol. Transl. Res. *4*, 129. https://doi.org/10.4172/2476-2261.1000129.

39. Faubert, B., Boily, G., Izreig, S., Griss, T., Samborska, B., Dong, Z., Dupuy, F., Chambers, C., Fuerth, B.J., Viollet, B., et al. (2013). AMPK is a negative regulator of the Warburg effect and suppresses tumor growth in vivo. Cell Metab. *17*, 113–124. https://doi.org/10.1016/j.cmet.2012.12.001.

40. Askew, C., Sellam, A., Epp, E., Hogues, H., Mullick, A., Nantel, A., and Whiteway, M. (2009). Transcriptional regulation of carbohydrate metabolism in the human pathogen Candida albicans. PLoS Pathog. *5*, e1000612. https://doi.org/10.1371/journal.ppat.1000612.

41. Nishi, K., Park, C.S., Pepper, A.E., Eichinger, G., Innis, M.A., and Holland, M.J. (1995). The GCR1 requirement for yeast glycolytic gene expression is suppressed by dominant mutations in the SGC1 gene, which encodes a novel basic-helix-loop-helix protein. Mol. Cell Biol. *15*, 2646–2653. https://doi.org/10.1128/mcb.15.5.2646.

42. Santana, D.J., and O'Meara, T.R. (2021). Forward and reverse genetic dissection of morphogenesis identifies filament-competent Candida auris strains. Nat. Commun. *12*, 7197. https://doi.org/10.1038/s41467-021-27545-5.

43. Mayr, E.M., Ramírez-Zavala, B., Krüger, I., and Morschhäuser, J. (2020). A zinc cluster transcription factor contributes to the intrinsic fluconazole resistance of Candida auris. mSphere *5*. https://doi.org/10.1128/mSphere.00279-20.

44. Bravo Ruiz, G., Ross, Z.K., Gow, N.A.R., and Lorenz, A. (2020). Pseudohyphal growth of the emerging pathogen Candida auris is triggered by genotoxic stress through the S phase checkpoint. mSphere *5*, e00151-20. https://doi.org/10.1128/mSphere.00151-20.

45. Traven, A., and Naderer, T. (2014). Microbial egress: a hitchhiker's guide to freedom. PLoS Pathog. *10*, e1004201. https://doi.org/10.1371/journal.ppat.1004201.

46. Wolf, A.J., Reyes, C.N., Liang, W., Becker, C., Shimada, K., Wheeler, M.L., Cho, H.C., Popescu, N.I., Coggeshall, K.M., Arditi, M., and Underhill, D.M.

(2016). Hexokinase is an innate immune receptor for the detection of bacterial peptidoglycan. Cell *166*, 624–636. https://doi.org/10.1016/j.cell.2016.05.076.

47. Sanman, L.E., Qian, Y., Eisele, N.A., Ng, T.M., van der Linden, W.A., Monack, D.M., Weerapana, E., and Bogyo, M. (2016). Disruption of glycolytic flux is a signal for inflammasome signaling and pyroptotic cell death. Elife *5*, e13663. https://doi.org/10.7554/eLife.13663.
48. Chen, K.W., and Schroder, K. (2013). Antimicrobial functions of inflammasomes. Curr. Opin. Microbiol. *16*, 311–318. https://doi.org/10.1016/j.mib.2013.02.004.
49. Yabal, M., Calleja, D.J., Simpson, D.S., and Lawlor, K.E. (2019). Stressing out the mitochondria: mechanistic insights into NLRP3 inflammasome activation. J. Leukoc. Biol. *105*, 377–399. https://doi.org/10.1002/jlb.Mr0318-124r.
50. Gross, O., Poeck, H., Bscheider, M., Dostert, C., Hannesschläger, N., Endres, S., Hartmann, G., Tardivel, A., Schweighoffer, E., Tybulewicz, V., et al. (2009). Syk kinase signalling couples to the Nlrp3 inflammasome for anti-fungal host defence. Nature *459*, 433–436. https://doi.org/10.1038/nature07965.
51. Hise, A.G., Tomalka, J., Ganesan, S., Patel, K., Hall, B.A., Brown, G.D., and Fitzgerald, K.A. (2009). An essential role for the NLRP3 inflammasome in host defense against the human fungal pathogen Candida albicans. Cell Host Microbe *5*, 487–497. https://doi.org/10.1016/j.chom.2009.05.002.
52. van de Veerdonk, F.L., Joosten, L.A.B., Shaw, P.J., Smeekens, S.P., Malireddi, R.K.S., van der Meer, J.W.M., Kullberg, B.J., Netea, M.G., and Kanneganti, T.D. (2011). The inflammasome drives protective Th1 and Th17 cellular responses in disseminated candidiasis. Eur. J. Immunol. *41*, 2260–2268. https://doi.org/10.1002/eji.201041226.
53. Joly, S., Ma, N., Sadler, J.J., Soll, D.R., Cassel, S.L., and Sutterwala, F.S. (2009). Cutting edge: Candida albicans hyphae formation triggers activation of the Nlrp3 inflammasome. J. Immunol. *183*, 3578–3581. https://doi.org/10.4049/jimmunol.0901323.
54. He, W.T., Wan, H., Hu, L., Chen, P., Wang, X., Huang, Z., Yang, Z.H., Zhong, C.Q., and Han, J. (2015). Gasdermin D is an executor of pyroptosis and required for interleukin-1β secretion. Cell Res. *25*, 1285–1298. https://doi.org/10.1038/cr.2015.139.
55. Shi, J., Zhao, Y., Wang, K., Shi, X., Wang, Y., Huang, H., Zhuang, Y., Cai, T., Wang, F., and Shao, F. (2015). Cleavage of GSDMD by inflammatory caspases determines pyroptotic cell death. Nature *526*, 660–665. https://doi.org/10.1038/nature15514.
56. Sborgi, L., Rühl, S., Mulvihill, E., Pipercevic, J., Heilig, R., Stahlberg, H., Farady, C.J., Müller, D.J., Broz, P., and Hiller, S. (2016). GSDMD membrane pore formation constitutes the mechanism of pyroptotic cell death. Embo j *35*, 1766–1778. https://doi.org/10.15252/embj.201694696.
57. Liu, X., Zhang, Z., Ruan, J., Pan, Y., Magupalli, V.G., Wu, H., and Lieberman, J. (2016). Inflammasome-activated gasdermin D causes pyroptosis by forming membrane pores. Nature *535*, 153–158. https://doi.org/10.1038/nature18629.
58. Seider, K., Brunke, S., Schild, L., Jablonowski, N., Wilson, D., Majer, O., Barz, D., Haas, A., Kuchler, K., Schaller, M., and Hube, B. (2011). The facultative intracellular pathogen Candida glabrata subverts macrophage cytokine production and phagolysosome maturation. J. Immunol. *187*, 3072–3086. https://doi.org/10.4049/jimmunol.1003730.
59. Navarro-Arias, M.J., Hernández-Chávez, M.J., García-Carnero, L.C., Amezcua-Hernández, D.G., Lozoya-Pérez, N.E., Estrada-Mata, E., Martínez-Duncker, I., Franco, B., and Mora-Montes, H.M. (2019). Differential recognition of Candida tropicalis, Candida guilliermondii, Candida krusei, and Candida auris by human innate immune cells. Infect. Drug Resist. *12*, 783–794. https://doi.org/10.2147/idr.S197531.
60. Ding, X., Kambara, H., Guo, R., Kanneganti, A., Acosta-Zaldívar, M., Li, J., Liu, F., Bei, T., Qi, W., Xie, X., et al. (2021). Inflammasome-mediated GSDMD activation facilitates escape of Candida albicans from macrophages. Nat. Commun. *12*, 6699. https://doi.org/10.1038/s41467-021-27034-9.
61. Kasper, L., König, A., Koenig, P.A., Gresnigt, M.S., Westman, J., Drummond, R.A., Lionakis, M.S., Groß, O., Ruland, J., Naglik, J.R., and Hube, B. (2018). The fungal peptide toxin Candidalysin activates the NLRP3 inflammasome and causes cytolysis in mononuclear phagocytes. Nat. Commun. *9*, 4260. https://doi.org/10.1038/s41467-018-06607-1.
62. Lo, H.J., Köhler, J.R., DiDomenico, B., Loebenberg, D., Cacciapuoti, A., and Fink, G.R. (1997). Nonfilamentous C. albicans mutants are avirulent. Cell *90*, 939–949. https://doi.org/10.1016/s0092-8674(00)80358-x.
63. Olivier, F.A.B., Hilsenstein, V., Weerasinghe, H., Weir, A., Hughes, S., Crawford, S., Vince, J.E., Hickey, M.J., and Traven, A. (2022). The escape of Candida albicans from macrophages is enabled by the fungal toxin candidalysin and two host cell death pathways. Cell Rep. *40*, 111374. https://doi.org/10.1016/j.celrep.2022.111374.
64. Muñoz, J.F., Gade, L., Chow, N.A., Loparev, V.N., Juieng, P., Berkow, E.L., Farrer, R.A., Litvintseva, A.P., and Cuomo, C.A. (2018). Genomic insights into multidrug-resistance, mating and virulence in Candida auris and related emerging species. Nat. Commun. *9*, 5346. https://doi.org/10.1038/s41467-018-07779-6.
65. Shi, L., Salamon, H., Eugenin, E.A., Pine, R., Cooper, A., and Gennaro, M.L. (2015). Infection with Mycobacterium tuberculosis induces the Warburg effect in mouse lungs. Sci. Rep. *5*, 18176. https://doi.org/10.1038/srep18176.
66. Huang, L., Nazarova, E.V., Tan, S., Liu, Y., and Russell, D.G. (2018). Growth of Mycobacterium tuberculosis in vivo segregates with host macrophage metabolism and ontogeny. J. Exp. Med. *215*, 1135–1152. https://doi.org/10.1084/jem.20172020.
67. Gleeson, L.E., Sheedy, F.J., Palsson-McDermott, E.M., Triglia, D., O'Leary, S.M., O'Sullivan, M.P., O'Neill, L.A.J., and Keane, J. (2016). Cutting edge: Mycobacterium tuberculosis induces aerobic glycolysis in human alveolar macrophages that is required for control of intracellular bacillary replication. J. Immunol. *196*, 2444–2449. https://doi.org/10.4049/jimmunol.1501612.
68. Westman, J., Walpole, G.F.W., Kasper, L., Xue, B.Y., Elshafee, O., Hube, B., and Grinstein, S. (2020). Lysosome fusion maintains phagosome integrity during fungal infection. Cell Host Microbe *28*, 798–812.e6. https://doi.org/10.1016/j.chom.2020.09.004.
69. Li, D.D., Jawale, C.V., Zhou, C., Lin, L., Trevejo-Nunez, G.J., Rahman, S.A., Mullet, S.J., Das, J., Wendell, S.G., Delgoffe, G.M., et al. (2022). Fungal sensing enhances neutrophil metabolic fitness by regulating antifungal Glut1 activity. Cell Host Microbe *30*, 530–544.e6. https://doi.org/10.1016/j.chom.2022.02.017.
70. Johnson, C.J., Davis, J.M., Huttenlocher, A., Kernien, J.F., and Nett, J.E. (2018). Emerging fungal pathogen Candida auris evades neutrophil attack. mBio *9*, e01403-18. https://doi.org/10.1128/mBio.01403-18.
71. Langley, R.J., Tsalik, E.L., van Velkinburgh, J.C., Glickman, S.W., Rice, B.J., Wang, C., Chen, B., Carin, L., Suarez, A., Mohney, R.P., et al. (2013). An integrated clinico-metabolomic model improves prediction of death in sepsis. Sci. Transl. Med. *5*, 195ra95. https://doi.org/10.1126/scitranslmed.3005893.
72. Kamentsky, L., Jones, T.R., Fraser, A., Bray, M.A., Logan, D.J., Madden, K.L., Ljosa, V., Rueden, C., Eliceiri, K.W., and Carpenter, A.E. (2011). Improved structure, function and compatibility for CellProfiler: modular high-throughput image analysis software. Bioinformatics *27*, 1179–1180. https://doi.org/10.1093/bioinformatics/btr095.
73. Schindelin, J., Arganda-Carreras, I., Frise, E., Kaynig, V., Longair, M., Pietzsch, T., Preibisch, S., Rueden, C., Saalfeld, S., Schmid, B., et al. (2012). Fiji: an open-source platform for biological-image analysis. Nat. Methods *9*, 676–682. https://doi.org/10.1038/nmeth.2019.
74. Ruijter, J.M., Ramakers, C., Hoogaars, W.M.H., Karlen, Y., Bakker, O., van den Hoff, M.J.B., and Moorman, A.F.M. (2009). Amplification efficiency: linking baseline and bias in the analysis of quantitative PCR data. Nucleic Acids Res. *37*, e45. https://doi.org/10.1093/nar/gkp045.

75. Reuss, O., Vik, A., Kolter, R., and Morschhäuser, J. (2004). The SAT1 flipper, an optimized tool for gene disruption in Candida albicans. Gene *341*, 119–127. https://doi.org/10.1016/j.gene.2004.06.021.

76. Arras, S.D.M., and Fraser, J.A. (2016). Chemical inhibitors of non-homologous end joining increase targeted construct integration in cryptococcus neoformans. PLoS One *11*, e0163049. https://doi.org/10.1371/journal.pone.0163049.

77. Doerflinger, M., Deng, Y., Whitney, P., Salvamoser, R., Engel, S., Kueh, A.J., Tai, L., Bachem, A., Gressier, E., Geoghegan, N.D., et al. (2020). Flexible usage and interconnectivity of diverse cell death pathways protect against intracellular infection. Immunity *53*, 533–547.e7. https://doi.org/10.1016/j.immuni.2020.07.004.

78. Sprouffske, K., and Wagner, A. (2016). Growthcurver: an R package for obtaining interpretable metrics from microbial growth curves. BMC Bioinf. *17*, 172. https://doi.org/10.1186/s12859-016-1016-7.

STAR★METHODS

KEY RESOURCES TABLE

REAGENT or RESOURCE	SOURCE	IDENTIFIER
Antibodies		
Anti-Mouse IL1-beta antibody	R&D systems	Cat#: AF-401-NA; RRID: AB_416684
Anti-Caspase-1 (p20) (mouse), mAb (Casper-1)	AdipoGen	Cat#: AG-20B-0042-C100; RRID: AB_2755041
Anti-GSDMD antibody	Abcam	Cat#: Ab209845; RRID: AB_2783550
Goat Anti-Rabbit antibody, human ads-HRP	Southern Biotech	Cat#: 4010-05; RRID: AB_2632593
Anti-caspase-3 antibody	Cell signaling technology	Cat#: 9662; RRID: AB_331439
HRP conjugated beta-Actin (C4)	Santa Cruz Biotechnology	Cat#: sc-47778; RRID: AB_626632
Chemicals, peptides, and recombinant proteins		
Nourseothricin	GoldBio	Cat#: N-500
Calcofluor white stain	Sigma-Aldrich	Cat#: 18909
Fetal bovine serum	Serana	Cat#: FBS-AU-015
Penicillin-Streptomycin	Sigma-Aldrich	Cat#: P4333
Dimethyl Sulfoxide	Sigma-Aldrich	Cat#: D8418
CellTracker™ Green CMFDA dye	Thermo Fisher Scientific	Cat#: C7025; CAS:136832-63-8
DRAQ7	Abcam	Cat#: ab109202
Nigericin	Thermo Fisher Scientific	Cat#: N1495; CAS: 28380-24-7
Metformin hydrochloride	Sigma-Aldrich	Cat#PHR1084; CAS: 1115-70-4
Lipopolysaccharides	Sigma-Aldrich	Cat#: L6143
ECL: Immobilon Forte Western HRP Substrate	Merck Millipore	Cat#: WBLUF0500
Ambion™ DNase I (RNase-free) (mouse qPCR)	Thermo Fisher Scientific	Cat#: AM2222
RNA*later* ™ Stabilization Solution	Thermo Fisher Scientific	Cat#: AM7020
ABT-737	Active Biochem	Cat#: A-1002
S63845	Active Biochem	Cat#: A-6044
Pan Caspase OPH Inhibitor Q-VD, Non-omethylated	R&D systems	Cat#: OPH001-01M
Caspofungin	Sigma	Cat#: SML0425
RPMI 1640 medium, no glucose	Thermo Fisher Scientific	Cat#: 11879020; CAS: 1135695-98-5
D-(+)-Glucose	Sigma-Aldrich	Cat#: G8270; CAS: 50-99-7
L-Glutamine	Sigma-Aldrich	Cat#: G3126; CAS: 56-85-9
L-Arginine	Sigma-Aldrich	Cat#: A5006; CAS: 74-79-3
Sodium Acetate	BDH Analytical chemicals	Cat#: BDH10236; CAS: 127-09-3
Lactic Acid 90%	Merk	Cat#:1.00366.2500
D-(+)-Galactose	US Biological	Cat#: G1030; CAS: 59-23-4
D-(+)-Fructose	Sigma	Cat#: F0127
Trizol reagent	Invitrogen	Cat#: 15596026
DNase I (RNase-free) (macrophage qPCR)	Ambion	Cat#: AM2224
Superscript III (macrophage qPCR)	Invitrogen	Cat#: 18080093
Critical commercial assays		
Wizard® SV Gel and PCR Clean-Up System	Promega	Cat#: A9281
Mouse IL-1β/IL-1F2 ELISA kit	R&D Systems	Cat#: DY401
CytoTox 96® Non-Radioactive Cytotoxicity Assay kit	Promega	Cat#: G1780
L-Lactate Assay Kit (Colorimetric)	ABCAM	Cat#: ab65331
Amplex™ Red glucose/glucose Oxidase Assay Kit	Thermo Fisher Scientific	Cat#: A22189
SuperScript™ III First-Strand Synthesis System (mouse qPCR)	Thermo Fisher Scientific	Cat#: 18080051
NucleoSpin RNA purification kit	Macherey-Nagel	Cat#: 740955.50

(*Continued on next page*)

Continued

REAGENT or RESOURCE	SOURCE	IDENTIFIER
Experimental models: Cell lines		
Wild type iBMDMs: C57BL/6 Cre-J2 background	Gifted by Marco Herold, Walter and Eliza Hall Institute of Medical Research	N/A
Casp1$^{-/-}$;*Casp11*$^{-/-}$;*Casp12*$^{-/-}$; *Casp8*$^{-/-}$;*RIP3K*$^{-/-}$iBMDMs: C57BL/6 Cre-J2 background	Gifted by Marco Herold, Walter and Eliza Hall Institute of Medical Research	N/A
Experimental models: Organisms/strains		
Mouse: wild type C57BL/6J	Monash Animal Research Platform (Melbourne, Australia)	RRID: IMSR_JAX:000664
Mouse: *Nlrp3*$^{-/-}$C57BL/6J	Walter and Eliza Hall Institute of Medical Research	MGI ID:3721141
C. auris: 470121	Gift from Sarah Kidd; National Mycology Refence Center, Adelaide, SA, Australia	Clade I, Clinical isolate India
C. auris: B8441	CDC, Atlanta, USA	Clade I, Clinical isolate, Pakistan
C. auris: B11098	CDC, Atlanta, USA	Clade I, Clinical isolate, Pakistan
C. auris: B11220	CDC, Atlanta, USA	Clade II, Clinical isolate, Japan
C. auris: B11221	CDC, Atlanta, USA	Clade III, Clinical isolate, South Africa
C. auris: B11244	CDC, Atlanta, USA	Clade IV, Clinical isolate, Venezuela,
C. auris: 470121 Δ*tye7*::*SAT1* isolate 1	This study	YCAT1335
C. auris: 470121 Δ*tye7*::*SAT1* isolate 2	This study	YCAT1336
C. auris: 470121 Δ*gal4*::*SAT1* isolate 1	This study	YCAT1337
C. auris: 470121 Δ*gal4*::*SAT1* isolate 2	This study	YCAT1338
C. auris: B8441 Δ*tye7*::*SAT1* isolate 1	This study	YCAT1339
C. auris: B8441 Δ*tye7*::*SAT1* isolate 2	This study	YCAT1340
C. auris: B8441 Δ*al4*::*SAT1* isolate 1	This study	YCAT1341
C. auris: B8441 Δ*gal4*::*SAT1* isolate 2	This study	YCAT1342
C. auris: B8441 Δ*cdc19*::*SAT1*	This study	YCAT1343
Oligonucleotides		
qPCR and deletion primers, see Table S1	This study	N/A
Software and algorithms		
CellProfiler 2.1.1	(Kamentsky et al., 2011)[72]	N/A
ImageJ 2.0.0-rc-69	(Schindelin et al., 2012)[73]	N/A
GraphPad Prism 9.0.0	GraphPad Software, San Diego, California USA	N/A
LinReg software	(Ruijter et al. 2009)[74]	N/A
Growthcurver package	Rstudio, PBC, Boston, MA, USA	https://cran.rproject.org/web/packages/growthcurver/vignettes/Growthcurvervignette.html#output-metrics
Other		
MColorpHast™ pH universal indicator strips pH 0-14	MerkMillipore	Cat#:1.09535.001
NuPAGE ™ 4–12% Bis-Tris Gel	Invitrogen	Cat#: WG1402

RESOURCE AVAILABILITY

Lead contact

Further information and requests for reagents should be directed to and will be fulfilled by the lead contact, Ana Traven (ana.traven@monash.edu).

Materials availability

C. auris and *C. albicans* strains and mouse strains used in this study are detailed in the key resources table. Fungal mutant strains generated in this study are available from the lead contact upon request.

Data and code availability

- Numerical data used to construct figures are provided as Dataset S1. Changes made to images and videos are detailed in Table S2. Unedited microscopy images for all figures can be accessed, upon request, from the lead contact.
- This paper does not report original code.
- Any additional information required to re-analyse the data reported in this paper is available from the lead contact upon request.

EXPERIMENTAL MODELS

Candida strains and media

The strains used in this study are listed in Table S1. The *C. auris* Clade I isolate 470121 was generously gifted by Sarah E. Kidd from the National Mycology reference center (Adelaide, Australia) and is a clinical isolate obtain from Dr. Sharon Chen. The other *C. auris* clinical strains used in this study were obtained from the Center for Disease Control (CDC, Atlanta, USA). Details of the *C. auris* clinical isolates used in this study can be found in Table S1. The *C. albicans* clinical isolate was SC5314. For heat-killed *C. auris* 16-h cultures were diluted to 1 × 10^7 cells/ml and incubated for 3 h at 65°C. All strains were maintained on Yeast Extract – Peptone – Dextrose (YPD) media (1% yeast extract, 2% peptone, 2% glucose, 80 μg/mL uridine, with addition of 2% agar). Where overnight liquid cultures were required such as for macrophage infections or growth curve assays, a single colony of *Candida* from a freshly streaked YPD plate was inoculated into liquid YPD medium and grown for 18 h at 30°C. For liquid growth assays, overnight cultures of *C. auris* were diluted to OD_{600nm} of 0.1 in prewarmed bone marrow derived macrophage (BMDM) medium containing RPMI 1640 supplemented with 12.5 mM HEPES, 10% FBS, 20% L-cell conditioned medium (containing macrophage colony stimulating factor) and 100 U/ml of penicillin-streptomycin (Sigma) (complete RPMI media). For growth assays investigating the effects of different types and concentrations of carbon sources, BMDM medium was made up with RPMI 1640 medium lacking glucose (Thermo Fisher 11879020) and supplemented with glucose (10, 20 and 40 mM), galactose (40 mM) or mannose (40 mM). For yeast plate growth tests on various nutrient sources, 10-fold dilutions of yeast cultures were spotted on minimal Yeast Nitrogen Base (YNB) media was supplemented with 2% of either glucose, fructose, mannose, acetate or glycerol. For some growth assays, 0.5 μg/mL antimycin was supplemented to the plates.

Strain construction

The Δ*tye7* and Δ*gal4* mutant strains were generated from clade I strains 470121 and B8441, and the Δ*cdc19* mutant strain was generated in the B8441 strain. Mutants were produced by deletion of the open reading frame using the SAT1 flipper cassette,[75] conferring resistance to nourseothricin. Primers used to generate the knockout cassettes that enabled the generation of these mutants can be found in Table S2. Deletion mutants were selected on YPD media supplemented with 400 μg/mL nourseothricin. The mutants were generated by standard methods based on PCR and homologous recombination, however as *C. auris* has a lower rate of homologous recombination compared to other *Candida* species,[42] W7 Hydrochloride (5 μg/ml) was added to the growth culture for 6 h as detailed in,[76] to reduce non-homologous end-joining. All strains were confirmed by diagnostic PCR and primers used for this can be found in Table S2. Both parental strains 470121 and B8441 are prototrophic and nourseothricin sensitive.

Isolation of murine bone marrow derived macrophages (BMDMs) and human monocyte-derived macrophages (hMDMs)

Mice experiments for BMDM isolations were approved by the Monash University Animal ethics committee (approval numbers ERM14292 and ERM25488). Human blood isolation experiments were approved by the Monash University Human Ethics Committee (project 21685).

For BMDM preparations, tibia and femur were harvested from six to eight weeks old C57BL/6 mice obtained from the Monash Animal Research Platform. For experiments using *Nlrp3* $^{-/-}$ BMDMs, tibia and femur from *Nlrp3* $^{-/-}$ mice were obtained from James Vince and Seth Masters at the Walter and Elisa Hall Institute. Bone marrow containing monocytes was flushed from these bones using BMDM media (RPMI 1640 supplemented with 12.5 mM HEPES, 10% FBS, 20% L-cell conditioned medium and 100U/ml of penicillin-streptomycin) and allowed to differentiate into BMDMs for 5–7 days as previously described.[30]

For preparation of hMDMs, blood of healthy volunteers was used to isolate PBMCs by Histopaque-1077 (Sigma-Aldrich) density gradient centrifugation. Using the Pan Monocyte Cell Isolation (Miltenyi Biotech) magnetic labelling system, CD14 and CD16-expressing monocytes were purified from the PBMCs. This enriched monocyte fraction was differentiated to macrophages (hMDMs) in a 25 cm^2 culture flasks in RPMI 1640 media containing 15 mM HEPES, 10% fetal bovine serum (Serana, Fisher Biotech), 100 U/ml penicillin-streptomycin (Sigma-Aldrich) and 50 ng/mL macrophage colony stimulating factor (M-CSF, R&D Systems) and incubated at 37°C in 5% CO_2 for 7 days.

METHOD DETAILS

Live cell imaging

For seeding macrophages in live cell imaging experiments, cells were gently scraped from petri dishes using a cell scraper (BD Falcon) and seeded in tissue culture-treated plates at a density of 1×10^5 cells/well in a 96-well tray and incubated overnight at 37°C + 5% CO_2. Live cell imaging procedure was followed as described in.[30] Briefly, macrophages were stained with 1 mM CellTracker Green CFMDA dye (ThermoFischer C7025) for 35 min in serum-free RPMI 1640 supplemented with 12.5 mM HEPES, 20% L-cell conditioned medium and 100 U/ml of penicillin-streptomycin (Sigma). Macrophages were then infected with *C. auris* at a multiplicity of infection (MOI) of 3:1 or 6:1 (yeast to macrophages) in BMDM medium and co-incubated for 1 h, followed by removal of non-phagocytosed yeast by washing with PBS. Where indicated, BMDM media was supplemented with arginine, glutamate, acetate, pyruvate, sorbitol or glucose at the concentrations indicated in the figures. For experiments investigating the effects of glucose concentrations, BMDM media was prepared with RPMI 1640 medium lacking glucose (Thermo Fisher 11879020) and 10% FBS. This media was used as un-supplemented ("no glucose") or supplemented with 10, 20 or 40 mM glucose. Where indicated, 125 ng/mL caspofungin was added post co-infection. For spike in experiments either 10 mM glucose, 10 mM pyruvate or 125 ng/mL caspofungin were added to the infection and control wells at 6 h post infection, and imaging was continued to 24 h. For experiments involving calcofluor inhibition of growth of non-phagocytosed *C. auris*, both infection and control conditions were treated with BMDM media containing 25 μg/mL calcofluor for 1 h post infection. Following this, each well of the assay plate was replaced with fresh BMDM media and imaged as above for 24 h. For experiments involving metformin, macrophages were pre-treated with 5 mM metformin for 24 h and then switched to fresh media with or without metformin prior to infection with *C. auris*. Uninfected macrophage controls were treated similarly. For experiments involving Quinoline-Val-Asp-Difluorophenoxymethylketone (QVD), macrophages were pre-treated with 10 μM QVD for 1 h and then switched to fresh media with or without metformin prior to infection with *C. auris*. Uninfected macrophage controls were treated similarly. After *C. auris* challenge treatment and control wells were replaced with media with and without 10 μM QVD for the remaining duration of the experiment. All media conditions also contained 0.6 mM DRAQ7 (Abcam) for tracking macrophage membrane permeabilization. Imaging was performed on a Leica AF6000 LX epifluorescence microscope (20x objective). The imaging data was analyzed and quantified using MetaMorph (Molecular Devices) and CellProfiler 2.1.1[72] as previously described[30,63] and plotted using Prism 9.0 (GraphPad Software, San Diego, California USA) software. ImageJ software[73] was used to compile live cell imaging time course images into movies.

For experiments with hMDMs, cells were detached in PBS with 2 mM EDTA and 2% FBS by incubating for 10 min at 37°C in 5% CO_2. This was followed by repeated rinses using a 10 mL syringe and 18G needle. The detached hMDMs were then seeded at a density of 5×10^4 cells/well of a 96-well plate, in RPMI 1640 media supplemented with 15 mM HEPES, 10% fetal bovine serum (Serana, Fisher Biotech), 100 U/ml penicillin-streptomycin and incubated at 37°C and 5% CO_2 overnight before infection. hMDMs were stained with 1 mM CellTracker Green CFMDA dye (ThermoFischer C7025) for 30 min prior to infection as above for BMDMs. After staining, hMDMs were primed in RPMI 1640 supplemented with 15 mM HEPES, 10% and 50 ng/mL lipopolysaccharide (LPS, Sigma) and incubated at 37°C and 5% CO_2 for 2 h for priming. After priming hMDMs were challenged with *C. auris* (strain 470121) at MOI of 6 for 1 h and the remaining procedures for live cell imaging were as described above for BMDM experiments.

For live cell experiments involving C57BL/6 Cre-J2 immortalised bone marrow-derived macrophages (iBMDM),[77] wild type and mutant cell lines deficient for caspase-1, caspase-11, caspase-12, caspase-8 and Receptor-Interacting Protein Kinase 3 (RIPK3) (negative for pyroptosis, necroptosis and extrinsic apoptosis) were passaged in DMEM supplemented with 10% FBS, 100U/ml of penicillin-streptomycin at 37°C and 5% CO_2. For imaging, cells were gently scraped from petri dishes using a cell scraper (BD Falcon) and seeded in tissue culture-treated plates at a density of 1×10^5 cells/well in a 96-well tray and incubated overnight at 37°C and 5% CO_2. The iBMDM macrophages were challenged with *C. auris* at MOI of 3:1. Live cell experimental procedure, imaging and analysis were carried out as described above for BMDM experiments.

Collection of supernatants and lysates for IL-1® ELISA, lactate dehydrogenase (LDH) and western blot assays

The seeding of macrophages was performed as described in live cell imaging methods. All assays were carried out in 24-well microplates and macrophages were seeded at 5×10^5 cells/well in BMDM media. Macrophages were primed with 50 ng/mL Lipopolysaccharide (LPS) for 3 h in fresh media, followed by either challenge with *C. auris* (strain 470121, MOI 6), *C. albicans* (strain SC5314 MOI 3) or uninfected for 1 h at 37 °C and 5% CO2. After this, cells were washed 3x in PBS to remove non-phagocytosed fungal cells, replenished with 250 μL fresh BMDM media and incubated for 3, 10 and 16 h. The 1-h time point was sampled directly after infection incubation. Treatment with 10 μM nigericin for 3 h was used as a positive control. Nigericin induces potassium efflux via H^+/K^+antiport across cell membranes, thus activating the NLRP3 inflammasome (Armstrong et al. Front Immunol 2019). For experiments looking at caspase-3 cleavage, ABT737 (1 μM) + S63845 (10 μM) treatment for 2 h was used to activate intrinsic apoptosis as a positive control. For each time point, supernatants were collected for ELISA (100 μL), Western blot (75 μ) and LDH assay (75 μL). ELISA and LDH assay supernatants were stored at −80°C. Western blot supernatants were mixed with 25 μL 4x sample buffer (RSB; ThermoFisher) with 5% ®-mercaptoethanol in microfuge tubes, boiled at 95 °C for 10 min and frozen at −20 °C. After collection of the supernatants, 150 μL of 1x RSB buffer with 2.5% ®- mercaptoethanol was added to each well and a 1 mL pipette tip was used to scrape cells for lysate faction. This was transferred to 1.5 mL microfuge tubes, boiled at 95 °C for 10 min and frozen at −20 °C.

IL-1β ELISA

The IL-1β levels in supernatant samples were measured using the Mouse IL-1β/IL-1F2 ELISA kit (R&D Systems, DY401), according to the manufacturer's instructions. Optical density measurements reflective of IL-1β levels were measured at 450 nm (with a wavelength correction of 540 nm) using a Tecan infinite M200 plate reader. Using the reference of IL-1β standards provided in the kit, an interpolated standard curve was generated in Graphpad Prism 9.0 (GraphPad Software, San Diego, California USA) to determine IL-1β levels for each sample.

LDH assay

The LDH levels in supernatant samples were measured using the CytoTox 96 Non- 23 Radioactive Cytotoxicity Assay (Promega, G1780) according to the manufacturer's instructions. Optical density measurements reflective of LDH levels were measured at 492 nm using a Tecan Spark 10M plate reader. LDH levels for each sample were quantified as fold change relative to the 10 μM nigericin positive control.

Western blot

For IL-1β, caspase 1 and gasdermin D Western blots, cell lysates and/or supernatants were boiled for 10 min at 95°C prior to loading, followed by loading onto 4–12% Bis-Tris NuPAGE protein gels (Invitrogen), SDS-PAGE and transfer onto nitrocellulose membrane (Millipore). Membranes were stained with Ponceau. Blocking was performed with 5% (v/v) skim milk in PBS-Tween (0.1% (v/v)) for 1 h, followed by probing with primary antibodies: anti-IL-1β (R&D, #AF-401-NA), anti-caspase-1 (Adipogen, AG-20B-0042-C100) and anti- GSDMD (abcam, ab209845). Incubations with primary antibodies (1:1000 dilution) were done overnight in a rotating wheel at 4°C, followed by washing in PBS-T and adding HRP-conjugated secondary antibodies (1:10,000 dilution) for 1 h at room temperature. Membranes were developed using Immobilin Forte Western HRP (Merck) and imaged using ChemiDoc MP system (BioRad). Analyses was performed using Image Lab and Adobe Illustrator.

For the caspase 3 Western blots, whole cell lysates were heated for 10 min, cooled then centrifuged prior to gel loading. For each sample, 20 μL was loaded onto 4–12% NuPage Bis-Tris gels in MES gel running buffer and SDS-PAGE was performed at 90 V for 10 min, followed by 120V for 1.5 h. Proteins were transferred onto PVDF-E membrane at 100 V for 1 h at 4°C. Following protein transfer, protein loading was assessed by ponceau staining, then the membrane was blocked in 5% skim milk powder in TBS-T for 30 min. Membranes were subsequently washed 3x in TBS-T for 5 min, then incubated in 5% BSA in TBS-T containing unconjugated anti-caspase-3 (CST9662, 1:1000 dilution) antibody overnight at 4°C, or in 5% skim milk powder in TBS-T containing HRP-conjugated anti-Actin (sc47778, 1:10,000) for 1 h at room temperature. Following this, membranes were washed twice in TBS-T, then incubated in 5% skim milk powder in TBS-T containing HRP-conjugated anti-rabbit antibody (1:10,000) for 1 h at room temperature. Membranes were then washed five times in TBS-T and subjected to ECL development and detection using the ChemiDoc MP system (BioRad). Images were processed using BioRad ImageLab and prepared in AffinityDesigner.

Lactate assay

The seeding of macrophages was as described in live cell imaging methods and assays were carried out in 96-well microplates with macrophages seeded at 1×10^5 cells/well in BMDM media. Macrophages were either challenge with *C. auris* (strain 470121, MOI 6) or uninfected for 1 h at 37 °C and 5% CO2. Following the 1-h infection, cells were washed thrice in PBS, replenished with 150 μL fresh BMDM media and incubated for 10 and 24 h. The 1-h time point was sampled directly after infection. At each time point, the supernatant was removed, plates washed 4 times in cold PBS and cells harvested in 4x Lactate Assay buffer (about 200 μL). For lactate level measurements *in vitro*, *C. auris* strain 470121 was cultures as for live cell imaging and grown for 1, 10 and 24 h in BMDM media. Yeast cells were harvested at each time point and subject to preparation for lactate assay as above. The processing of samples and lactate level measurement procedure were followed as specified in the L-Lactate Assay Kit (Colorimetric) (ABCAM – ab65331) according to the manufacturer's instructions. Optical density was measured at 450 nm using a Tecan Spark 10M plate reader. Using the reference of lactate standards provided in the kit, an interpolated standard curve was generated in Graphpad Prism 9.0 (GraphPad Software, San Diego, California USA) to determine lactate levels for each sample.

Quantification of glucose

To quantify glucose in *C. auris*-macrophage infection assays, supernatant was collected at 1, 4, 8 10 and 24 h from macrophages (96-well microplates seeded at 1×10^5 cells/well) either challenge with *C. auris* (strain 470121, MOI 6) or uninfected. Glucose levels were measured using the Amplex Red glucose/glucose Oxidase Assay Kit (Thermo Fisher A22189) according to the manufacturer's instructions. Optical density measurements were carried out at 450 nm using a Tecan Spark 10M plate reader.

Colony forming unit (CFU) measurements

For counting CFUs, macrophages were seeded as described in live cell imaging methods. All assays were carried out in 24-well microplates and macrophages were seeded at 2.5×10^5 cells/well in BMDM media. *C. auris* cultures were grown over night for 18 h in YPD medium at 30°C. The next day macrophages were challenged with *C. auris* (MOI 3 for 1 h). Cells were then washed 3x in PBS, replenished with 250 μL fresh BMDM media and incubated for 2, 4, 8 and 10 h. At each time point supernatant was removed and saved, and macrophages were lysed with ice-cold distilled water to obtain intracellular *C. auris*.

For calcofluor white inhibition assay the *C. auris* 470121 strain was cultured as for live cell imaging in BMDM media either with or without 25 μg/ml calcofluor white and grown for a further 1 h at 30°C, followed by three washes in PBS. For all CFU experiments, appropriate dilutions of supernatant (extracellular *C. auris*) and lysate (intracellular *C. auris*) were plated on YPD plates and incubated for 2 days at 30 °C to count yeast colonies.

pH measurements of media

To measure the pH of medium during *C. auris*-macrophage infection, experiments were prepared as detailed in live cell imaging. MColorpHast pH universal indicator strips at a range of pH 0–14 (MerkMillipore) was used to dip into infection wells at 1 h and then again at 24 h after infection had progressed. Color changes were compared to provided key to determine pH range.

Growth curves

For growth curve assays WT, Δ*tye7*, Δ*gal4* and Δ*cdc19* strains were cultured as described in the candida strains and media method. Assays were run in either BMDM media or BMDM media with 10 mM glucose or acetate. A matched media only controls were also run alongside the *C. auris* samples. Assay was conducted in 200 μL volumes of a 96-well plate. Growth was determined by optical density measurements at 600 nm using a Tecan Spark 10M plate reader over a 24-h period. For growth curves to determine the effect of metformin on *in vitro C. auris* growth, assay set up was the same as above for the 470121 strain and was run in BMDM media with or without 5 mM metformin.

Doubling times for WT, ⊗Δ*tye7*, Δ*gal4* were calculated using Growthcurver package in Rstudio (https://cran.rproject.org/web/packages/growthcurver/vignettes/Growthcurvervignette.html#output-metrics).[78]

Phagocytosis determinations

Rates of *C. auris* phagocytosis by macrophages were calculated using images captured from experiments shown in Figure 1A. Briefly, a random sampling of macrophages in a fixed area was used in counts from images for three independent repeats. More than 100 macrophages were counted for each replicated and included both *C. auris*-infected and uninfected cells. The number of *C. auris* in each macrophage was counted. The phagocytic ratio was calculated by dividing the total number of counted *C. auris* by the total number of macrophages. The data from the 3 independent experiments is presented in Dataset S1.

Quantitative PCR analysis (qPCR)

Primers used for qPCR are detailed in Table S2. For RNA isolation in *C. auris*/macrophage infections BMDMs were seeded at a density of 1×10^6 cells/well in a 6-well tray, and then infected with *C. auris* at a MOI of 6 in BMDM medium. After 1 h of co-incubation and PBS washes, media was replaced for each well with fresh BMDM medium. Macrophage samples without *C. auris* infection (control samples) were treated in the same way. Samples were incubated for 1, 4, 8 and 10 h. At the given time points, samples were harvested using Trizol reagent to lyse the cells. The lysate was centrifuged to separate the *Candida* pellet from the macrophage RNA supernatant in the infected samples. RNA from all samples was isolated using the Trizol method. Reverse transcription was carried out on 1 μg of DNase I (Ambion)-treated total RNA using Superscript III cDNA kit (Invitrogen). Quantitative PCR was performed on a LightCycler 480 (Roche) using the FastStart Universal SYBR Green Master Rox (Roche) master mix. Data analysis was carried out using the LinReg software[74] and macrophage glycolytic gene expression was normalised to *18S* rRNA levels. Two technical repeats were averaged for one biological repeat.

For qPCR experiments assessing *C. auris* glycolysis gene expression, yeast cultures were grown *in vitro* at 37 °C. Overnight cultures were diluted to OD_{600nm} 0.1 in BMDM media and grown at 37 °C for 7 h. Total RNA was isolated using the hot phenol method and DNAse treatment, reverse transcription, qPCR method and data analysis were carried out as described above. *RDN25* transcript levels were used for normalisation. The *RDN25* gene encodes for 25S ribosomal RNA and maintains consistent levels of expression across conditions and strain backgrounds, making it suitable as a control gene. Two technical repeats were averaged to obtain the biological repeat.

For experiments measuring gene expression in kidneys of mice infected with *C. auris*, mice were infected in groups of five with 1×10^7 of the wild type and Δ*tye7 C. auris* strains by lateral tail injection. After 48 h, mice were culled, and kidneys were excised aseptically and stored in RNA*later* solution (Thermo Fischer). RNA extraction was done using NucleoSpin RNA purification kit (Macherey-Nagel). Reverse transcription was performed using qScript cDNA synthesis kit (Quanta Biosciences, Beverly, MA) on a C1000 thermal cycler (Bio Rad) with the following settings: 1 cycle, 22°C, 5 min; 1 cycle, 42°C, 30 min; 1 cycle, 85°C, 5min; 4°C hold. The qPCR was done using SyGreen Blue Mix (PCRBiosystems, London, UK), and primer pairs for *Glut1*, *Hk2* and *Pfkfb3* (Table S1) on a QuantStudio 5 machine (Applied Biosystems) with PCR settings were: 95°C, 2 min; 40 cycles: 95°C, 5 s, 60°C, 20 s. The *18s* transcript levels were used for normalization. Relative gene expression was calculated using the △△Ct method.

Animal infections

Six-week old female BALB/c mice weighing 18 to 22 g were purchased from Envigo, Rehovot, Israel. Animal experiments were reviewed and authorized by the Tel Aviv Sourasky Medical Center Institutional Animal Care and Use committee (permit number TLVMC – IL – 2112–124 – 3). Mice were housed in filter topped cages and fed autoclaved food and water. *C. auris* wild type and Δ*tye7* strains were grown in liquid yeast-extract agar glucose medium (YAG; yeast extract at 5 g/L; glucose at 10 g/L; agar at 15

g/L; 1 M $MgCl_2$ at 10 mL/L; trace elements at 1 mL/L) in a shaking incubator at 30°C, washed twice in sterile PBS, and resuspended in PBS at a concentration of 10^8 cells/ml (inoculum suspension). For each tested *C. auris* strain, mice were infected in groups of 7 with 10^7 yeast cells in 100 μL PBS by lateral tail vein injection. Mice were euthanized using CO_2 inhalation 48 and 120 h after infection. Kidneys were excised aseptically, weighed, and homogenized in 1 mL sterile PBS. Homogenates were serially diluted in PBS, plated on YAG and incubated at 30°C for 48 h. CFU counts were used to calculate the tissue fungal burden (CFU/g).

QUANTIFICATION AND STATISTICAL ANALYSIS

Statistical analyses were conducted in Graphpad Prism 9.0 (GraphPad Software, San Diego, California USA) and are detailed in each of the figure legends. One-or two-way ANOVA Bonferroni's multiple comparison tests were conducted on CFU counts, LDH assays, Lactate level assay, IL-1β assay, ELISA experiments and qPCR experiments. Kruskal Wallis non-parametric test and the Dunn's multi comparison test was conducted on the fungal qPCR assay and assays determining fungal burden in animal infection. For all experiments a p value of less than 0.05 was considered to be statistically significant.